

Vortices Shed by Accelerating Flat Plates

M. Matjoi

A dissertation submitted to the Faculty of Engineering and the Built Environment,
University of the Witwatersrand, Johannesburg, in fulfilment of the requirements for the
degree of Master of Science in Engineering

Johannesburg, May 2017

Declaration

I declare that this dissertation is my own, unaided work, except where otherwise acknowledged. It is being submitted for the degree of Master of Science in Engineering in the University of the Witwatersrand, Johannesburg. It has not been submitted before for any degree or examination at any other university.

Signed this 25th day of May 2017

A handwritten signature in black ink, appearing to read 'Matjoi', with a stylized flourish at the end.

M. Matjoi

Acknowledgments

A heartfelt and sincere thank you to my supervisors, Professor B. W. Skews and Mr. R. Paton, for guiding me and securing funding for this project.

I would like to thank Dr. I. Gledhill and Mr. C. Mahlase, from Ledger Fluxion, for funding this project.

Thanks are extended to my former colleagues, Bright Ndebele and Russell Hall, for their assistance with the experimental set-up and some software used in the project.

I would like to thank Mr. O. Mvudi for introducing me to Star CCM+. I would also like to thank Mr. C. de Wet from Aerotherm and Dr. S. Hooseria from CSIR, for their quick responses to my emails when I had questions related to Star CCM+.

I would also like to thank Mr. S. Riekert and the rest of Wits mechanical engineering workshop team for assisting with the manufacturing of the parts for experimental set-up.

To all my friends and family that helped, encouraged and motivated me to complete this thesis.

Abstract

Flow around flat plates that were uniformly accelerated from rest with acceleration of 13g is analysed with overset mesh from Star CCM+ commercial CFD software. The particular interest is more on the vortices shed from the plate edges. Three 8mm thick plates of the same cross-sectional areas (108mm length equilateral triangular, 71mm length square and 80mm diameter circular) were simulated. The validation of the numerical method was achieved by using laser vapor sheet method to visualize the flow profiles of accelerating circular plate and comparing the CFD and experimental results. The CFD and experimental results were consistent with each other.

It was found that when a plate accelerated in air, it displaced air particles out of its way. The shear layers of air separated from the front edges of the plate and rolled around a vortex core forming a primary vortex ring in the plate wake. The size of the primary vortex increased with Reynolds number (Re) that was increasing with time. This was because as Re increased, more fluid particles were displaced from the front face of the plate at a time. More displacement of the fluid particles led to shear layers separating from the plate edges with stronger momentum resulting in larger vortex ring. The shape of the primary vortex depended on the shape of the accelerating plate. For the circular plate, all the points on the front edge being equidistant from the plate centroid, fluid particles were evenly displaced from that separation edge. The result was an axis-symmetric ring of primary vortex around a circular vortex core. The asymmetric plates (triangular and square) did not evenly displace air particles from their edges of separation. The result was an asymmetric vortex ring. More air particles separated from the plate at separation points closest to the plate centroid and led to the largest vortical structure there. That is; the primary vortex ring was largest at the midpoints of the plate edges because they were the closest points of separation from the plate centroid. The size of the primary vortex continuously reduced from the mid-points of the plate edges to the corners. The corners had the smallest primary vortical structure due to being furthest points of separation from the plate centroid. The parts of the vortex ring from the two edges of the plate interacted at the corner connecting those edges.

Key words: Accelerating plates, CFD, Laser Vapour Sheet, Separation points, Vortex shedder, shear layer

Table of contents

Declaration.....	ii
Acknowledgments.....	iii
Abstract.....	iv
Table of contents.....	vi
List of tables.....	viii
List of figures.....	ix
Nomenclature.....	x
Chapter 1: Introduction.....	1
1.1. Background and motivation.....	1
1.2. Research aim.....	3
1.3. Objectives.....	3
1.4. Outline.....	4
Chapter 2: Literature review.....	5
2.1. Vortex shedding.....	5
2.2. Acceleration effects in external aerodynamics.....	6
2.2.1. Vortex shedding from an accelerated plate.....	6
2.2.2. Acceleration effects in other bodies rather than flat plates.....	6
2.3. Aerodynamic effect of changing a cross-section of a bluff Body.....	7
2.4. Computational fluid dynamics.....	8
2.4.1. CFD method used for simulation of accelerating plates.....	8
2.4.2. Modelling turbulent flows.....	9
2.5. Experimental Flow Visualization.....	10
Chapter 3: Experimental Method.....	12
3.1. Introduction.....	12
3.2. Experimental Set-up.....	12
3.3. List of Apparatus.....	15
3.4. Procedure for Capturing Images of Flow Profiles.....	16
3.5. Procedure for Determining the Experimental Acceleration.....	17
Chapter 4: CFD method used.....	18
4.1. Problem Description.....	18
4.2. Geometry and Boundary Conditions.....	19
4.3. Meshing.....	22
4.4. Physics of uniformly accelerated plate from rest.....	26
Chapter 5: Results and discussion.....	29
5.1. Calculation of experimental acceleration of a circular plate.....	29
5.2. Results of vortices shed by accelerating circular Plate.....	32
5.2.1. Validation of results for accelerating circular plate.....	32
5.2.2. Development of the vortices around an accelerating circular plate.....	38
5.2.3. Summary of vortices shed by accelerating circular plate.....	44
5.3. Results of vortices shed by accelerating triangular plate.....	44
5.3.1. Validation of results for accelerating triangular plate.....	44
5.3.2. Development of the vortices around an accelerating triangular plate.....	45
5.3.3. Vortex behavior from the mid-points to the triangular plate corners.....	51
5.3.4. Summary of vortices shed by an accelerating triangular plate.....	52
5.4. Results of vortices shed by accelerating square plate.....	53

5.4.1.	Validation of results for accelerating square plate.....	53
5.4.2.	Development of the vortices around accelerating square plate	54
5.4.3.	Behavior of vortex from the mid-points to the corners of the square plate	60
5.4.4.	Summary of vortices shed by accelerating square plate	62
5.5.	Drag force from accelerating plates	63
5.6.	Experimental Challenges	65
5.7.	Computational Challenges	67
Chapter 6: Conclusion and recommendation		68
6.1.	Conclusion	68
6.1.1.	Accelerating plates in general	68
6.1.2.	Accelerating axis-symmetric plates	69
6.1.3.	Accelerating non-axis-symmetric plates.....	69
6.2.	Recommendations.....	70
<i>References</i>		71
<i>Appendix</i>		74
Appendix 1: Specifications for the apparatus used.....		74
Appendix 2: Triggering circuit and program code for triggering a high speed camera		76
Appendix 3: Estimating the acceleration.....		79

List of tables

Table 1: Some constants of accelerating plate at final time step	19
Table 2: Mesh information.....	24
Table 3: Estimation of circular plate acceleration	31
Table 4: Pressure regulator specification [42]	74
Table 5: Vacuum pump specification	74
Table 6: Electro-magnet specification [42].....	74
Table 7: Electro – magnet control chunk specification [42].....	74
Table 8: 2W – Laser specification	75
Table 9: FSR specification [39]	75
Table 10: Photron FASTCAM SA5 high speed camera specification [42].....	75
Table 11: Data for accelerating circular plate.....	80

List of figures

Figure 1: Vortex core (yellow) and streamlines (blue) from a delta wing [15].....	5
Figure 2: High level diagram of the experimental set-up	13
Figure 3: The experimental rig system for accelerating plates	14
Figure 4: Cutting the domain for simulation from the experimental set-up	19
Figure 5: Geometry and boundary conditions for simulation of accelerating plates	20
Figure 6: Plates that were simulated	22
Figure 7: Example of the generated mesh at final Re	25
Figure 8: Diagram explaining how displacement versus time graph data was recorded..	30
Figure 9: Displacement versus time graph of accelerating circular plate	31
Figure 10: Trial 1: experimental results (left) versus CFD results (right) at xy plane for accelerating circular plate	34
Figure 11: Trial 2: experimental results (left) versus CFD results (right) at xy plane for accelerating circular plate	35
Figure 12: Trial 3: experimental results (left) versus CFD results (right) at xy plane for accelerating circular plate	36
Figure 13: Comparison of the experimental (left) and CFD (right) results at final Re (27505) and xy plane for accelerating circular plate	37
Figure 14: Development of vortices from accelerating circular plate at xy plane.....	40
Figure 15: Behavior of 3D vortex core around accelerating circular plate.....	42
Figure 16: 3D development of vortices around accelerating circular plate	43
Figure 17: Development of vortices from accelerating triangular plate at xy plane	45
Figure 18: Different points of separation around the triangular plate	46
Figure 19: Behavior of 3D vortex core around accelerating triangular plate	48
Figure 20: 3D development of vortices around accelerating triangular plate.....	50
Figure 21: Different views of 3D iso-surfaces of vorticity around a triangular plate at final Re (27505)	51
Figure 22: Development of vortices around accelerating square plate at xy plane	54
Figure 23: Different points of separation around the square plate.....	55
Figure 24: Behavior of 3D vortex core around accelerating square plate	57
Figure 25: 3D development of vortices around accelerating square plate.....	59
Figure 26: Showing 3D interactions of vortex ring from the edges of a square plate at the corner Re (27505)	60
Figure 27: Different views of 3D iso-surfaces of vorticity around a square plate at final Re (27505)	61
Figure 28: Pressure differential between the front and rear faces of accelerating plates .	64
Figure 29: Drag force of accelerating plate versus time	65
Figure 30: Fine and uniform smoke not producing clear and visible vortices (left) and smoke with turbulence producing visible vortex (right).....	67
Figure 31: Photo of triggering circuit used	76

Nomenclature

a_p	Plate uniform acceleration in (m/s^2)
CFD	Computational Fluid Dynamics
FE	Front edges; edges on the plate side which has a shaft
FF	Front face; plate face on the side with a shaft
FSR	Force sensing resistor
L_p	Length of the plate in (m)
LVS	Laser Vapour Sheet Visualisation method
Ma	Mach number
ρ	Fluid density in (kg/m^3)
Re	Reynolds number
RE	Rear edge; edge on the side of plate without shaft
RF	Rear face; plate on the side without shaft
S(t)	Displacement of the accelerating plate at time t in (m)
t	Time in (s)
μ	Dynamic viscosity in (kg/m.s)
V_{pf}	Plate final velocity in (m/s)
$V_p(t)$	Plate velocity at Time t in (m/s)

Chapter 1: Introduction

1.1. *Background and motivation*

In most studies of flow around bluff bodies, vortex shedding is analysed from bodies interacting with fluids at constant speeds. It is either the system that would be rotating at constant angular velocities or a stationary bluff body placed in a constant free stream [1]. As a result, the fluid-body interaction at uniform speeds is generally well understood in fluid dynamics.

The study that is still at infancy stages is that of flow around accelerating vortex shedders or bluff bodies. An aerodynamic body would not reach a constant velocity without accelerating in one way or the other in real life. A lot of engineering applications experience acceleration effects. Before an aircraft can cruise at some constant speed, it has to go through acceleration during take-off. Consequently, there is a need to understand the effects of vortex shedding from such a plane on the the houses near the airports [2].

Moreover, the vortices shed by the protruding parts of an accelerating missile such as fins affect the stability of the missile. The acceleration effects are also found in transient flows behind starting and stopping turbomachineries like butterfly valves [3]. The unsteady separated flows that explains how “rotational forces on flapping wings stabilise the leading edge vortices to enhance lift production” [4] also fall under bodies interacting with fluids with non-uniform velocities.

Unlike constant velocity cases, Reynolds number evolves in time [5] during the acceleration of a vortex shedder due to velocity that is increasing with time. Therefore, there will be a unique shedding frequency at each instantaneous Reynolds number. The application involving acceleration is more unsteady and time history becomes very important. The simpler theory derived from constant frequency vortex shedders that is popular in fluid dynamics can not be applied in this more complex cases [6]. Vortex shedding in unsteady flows is not well understood [7]. Some of the challenges that might be delaying the study of flow around vortex shedders accelerating in compressible fluids are [8]:

- Mathematical complexity of modelling a body accelerating in a compressible fluid.

- Difficulties in experimentally measuring the transient effects caused by accelerating bodies (especially at high velocities) and
- Slow development of computational methods

The first two points are still very challenging to fluid dynamicists. The assumptions and simplifications in mathematical models can solve a fluid problem faster; but they also lead to inaccurate decisions when attempting to simplify complex problems. As far as the second challenge is concerned, performing experiments in an attempt to understand the flow profiles in some engineering applications can sometimes be costly, time-consuming and risky if not impossible [9]. Fluid dynamicists usually resort to performing experiments on small scale models. Then they use dimensional analysis and similarity laws to extrapolate the results onto full scale prototypes. The problem with this alternative is that there might be insufficient rules to relate a model and a full scale body; also, not all the features of the system can be simulated by the small scale models [9].

However, the fast development of computational fluid dynamics in the recent years has alleviated the last problem about CFD [8]. CFD simulations are cheaper and faster [10]. However, CFD cannot replace the experimental analysis of fluid dynamics problems because experiments provide the closest possible approximation of a physical reality [11]. Experimental results must be used to evaluate the numerical predictive code-performance before using such a code with confidence [12]. In short, experiments and CFD have to work in parallel in order to validate the numerical method being used to analyse complex fluid dynamics parameters like vortices shed by accelerating bluff bodies in air. The reason is that the advantages of one method can alleviate the limitations of the other one.

Flow over accelerating flat plates in air is a simplified model that can be used to investigate the transient or unsteady separated flows in a lot of engineering applications [3]. The study is not completely new. There are a few published papers about flow around flat plates being uniformly accelerated in a direction perpendicular to their flat faces. However, most of these studies are analysing the plates in 2D. There is still a vacuum to fill as far as the third coordinate in space (z -axis) is concerned

Briefly, the identification of the following loopholes in the study of flow around bluff bodies has led to the proposal of a 3D CFD method for visualizing vortices shed by rapidly accelerating flat plates:

- Limited investigation of acceleration effects in flow around bluff bodies; most studies focus on bodies moving with constant velocities in fluids.
- Wind tunnel being limited to small accelerations as “higher accelerations would lead to pressure gradients along the wind tunnel” [13]. It must also be noted that a body has to be stationary in a moving fluid in the wind tunnel and not vice versa.
- The few studies that investigate acceleration effects use 2D simulations (not 3D) which compromises the need for analysing flow features in all three coordinates in space (X, Y and Z).

1.2. Research aim

The aim of this research is to investigate flow around plates that were uniformly accelerated from rest with acceleration of 13g in 3D. The particular interest is on the vortices shed from the plate edges. Three 8mm thick plates of the same cross-sectional areas (108mm length equilateral triangular, 71mm length square and 80mm diameter circular) were analysed.

1.3. Objectives

In summary, the objectives of this project are as follows:

- Proposing a CFD method for simulating 3D flow around plates that were uniformly accelerated from rest with particular interest to the vortices they shed. Flat plates were simulated due to being cost and time effective to validate experimentally.
- Experimentally visualising flow around rapidly accelerating flat plates in order to validate the proposed CFD method. A high speed camera was used to experimentally visualise their flow profiles using the laser vapour sheet method.
- To investigate the effect of the geometry of a bluff body on the flow profile; formation and development of vortices from the plate edges of the same cross-sectional areas and thicknesses but with different shapes of cross-sections (circular, triangular and square) were compared.
- Overset meshing in Star CCM+ CFD commercial package was used for simulating flow around such flat plates in 3D.

1.4. Outline

The document has been divided into six chapters. Chapter one introduces, motivates and outlines the project. Chapter two reviews the literature relevant to the project. Experimental and numerical methodologies are treated in chapter three and four respectively. Chapter five focuses on the results and discussion before chapter six where conclusions reached are drawn and recommendations made based on those conclusions.

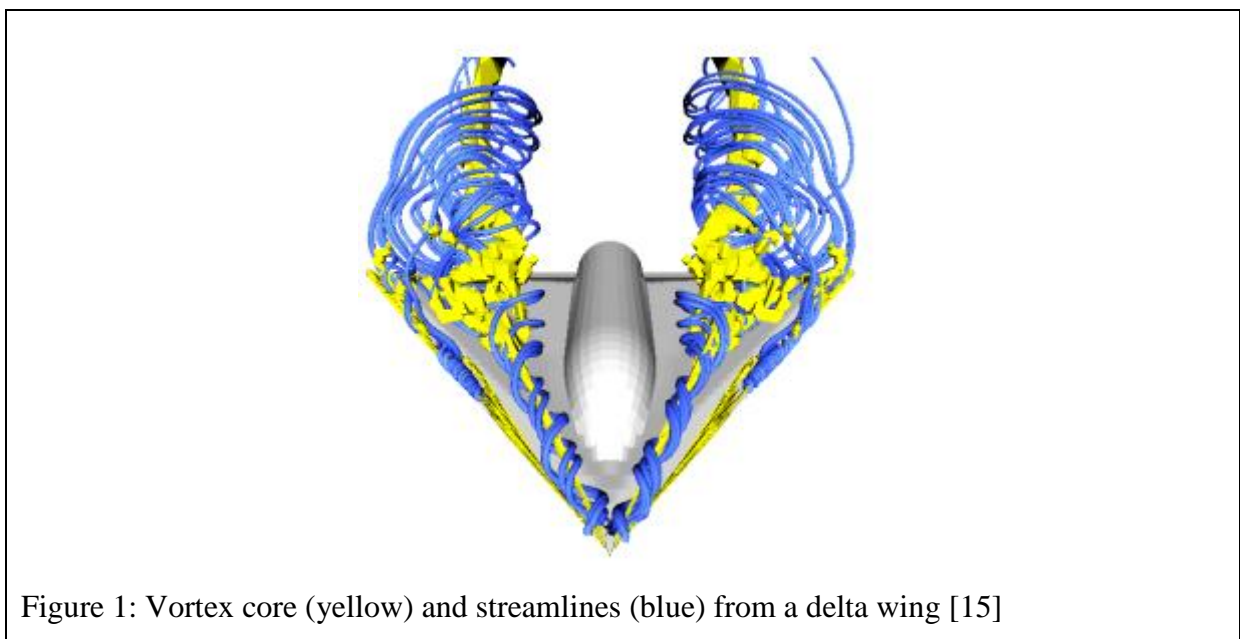
Chapter 2: Literature review

2.1. Vortex shedding

A vortex is defined as a “collective swirling motion of multiple fluid particles around a common center” [14]. However, this is just an intuitive definition derived from the natural swirling phenomena that are usually observed as in a tornado; coming up with a formal definition is still a challenge in fluid dynamics even today [15]. Although there is no formal definition of vortex, there are a few methods for vortex identification. These methods can be classified into [16]:

- Methods based on velocity gradient tensor
- Methods that rely on vorticity
- Lagrangian methods
- Others

Figure 1 below is an example of vortex identification around a delta wing.



A wake with vortices would have velocity and pressure fields that are unsteady in both space and time. Such flows are complex and therefore cannot be solved analytically like steady ones [6]. The study of start-up vortex began during the days of Prandtl [5]. There are pros and cons of vortex shedding. For example, inlet vortices can be damaging to the aircraft engines [17] while on the other hand, a wing can be flapped to prolong leading edge vortices to

improve the aerodynamic coefficients [4]. There are other many engineering applications where a good understanding of vortex dynamics is of vital importance to avoid the negative effects of shed vortices while on the other hand benefiting from their positive side.

2.2. Acceleration effects in external aerodynamics

2.2.1. Vortex shedding from an accelerated plate

Wang et. al., [3] simulated the transient flow generated from a started plate using a dynamic mesh based finite volume method in ANSYS Fluent. The problem was modelled as a 2D incompressible unsteady viscous flow. The fluid velocity on the surface was assumed to be equal to the velocity of the plate (no-slip boundary condition). For low accelerations, evolution of the vortices found for uniformly accelerated plate was similar to the numerical results of Koumoutsakos [18] who simulated the viscous flow normal to an impulsively started and uniformly accelerated flat plates. They observed the formation and development of a primary spiral vortex from the plate edges. The size of primary vortex increased during the accelerated plate motion.

Rosi and Rival [19] experimentally investigated entrainment and topology of accelerating shear layers from accelerating circular plate. They reached the following conclusions [19]:

- Increasing acceleration leads to increased shedding frequency.
- Increasing acceleration reduces the spacing of Kelvin Helmholtz (KH) instability.
- KH becomes clearer and more organised with increasing acceleration.

2.2.2. Acceleration effects in other bodies rather than flat plates

Gledhill et. al., [1] investigated acceleration effects on missile aerodynamics using CFD. Moving reference frames in the block-structured CFD-code EURANUS was used. The two important findings were that there was a significant effect of acceleration on the missile wave drag and movement of strake-generated vortices when the missile turns.

Lee et. al., [20] experimentally investigated free stream acceleration effects on drag force in bluff bodies using a wind tunnel. Compared to non-accelerated bodies, the additional momentum due to acceleration was found to always increase drag in bluff bodies with fixed separation points (i.e. square cylinder). The acceleration of air in the wind tunnel was about 3.6 m/s^2 . This acceleration is very low when compared to the accelerations of about 13g used

in the current project. The wind tunnel is usually limited to lower accelerations because “higher accelerations would lead to pressure gradients along the wind tunnel” [13].

Roohani and Skews [8] numerically compared the lift and drag forces from accelerating and constantly-moving aerofoils. In the subsonic region, acceleration was found to reduce lift and increase drag when compared to constantly-moving aerofoils. The reasoning behind lift behavior was that at a certain instantaneous Mach number of accelerating body, an equilibrium would not have been reached hence lower lift than in steady aerofoils that would be in equilibrium under the same range of Mach numbers. Higher drag values were attributed to more fluid inertia in accelerating bodies. Although the aerofoils are streamlined when compared to the bluff bodies studied by Lee et. al., [20], the results about drag were consistent in both studies. The additional momentum due to acceleration was found to always increase drag when compared to steady bluff bodies interacting with fluid at constant speeds.

2.3. Aerodynamic effect of changing a cross-section of a bluff Body

It has already been stated that most of the papers about a uniformly accelerated plates are in 2D. The analysis in 2D does not take all three coordinates in space (X, Y and Z) into account. In this dissertation, the effect of changing the shape of the plate was investigated in 3D. One of the important concepts in aerodynamics is aerodynamic efficiency; the ratio of lift over drag forces (L/D). Aerodynamic efficiency can be improved by increasing lift or reducing drag [21].

Altering the shape of a body has a significant impact on its aerodynamic performance. In the subsonic region, the total drag force experienced by a body is the sum of the skin friction and pressure drags [22]. This total drag can be altered by changing the shape of the body interacting with a fluid. The bluff bodies generally have more pressure drag than skin friction drag when compared to streamlined bodies [23]. This pressure drag usually leads to bluff bodies experiencing more overall drag than their streamlined counterparts. Altering the geometry of an aerodynamic body can contribute in reduction of the total drag. Drag reduction reduces fuel consumption and increases performances of the automobiles and aeronautics [22].

An example of investigating different geometries in an attempt to improve aerodynamic efficiency is the work of Mahjoob [21]. ANSYS Fluent CFD code with the standard k- ϵ

model was used to compare aerodynamic efficiencies of missiles with the same cross-sectional area but different geometries (circular and square cross section with round edges). Even though the square section missile had more friction drag, it was found to be producing less overall drag.

2.4. Computational fluid dynamics

2.4.1. CFD method used for simulation of accelerating plates

Per the knowledge of the author, there are two commercial CFD software at University of the Witwatersrand. Both ANSYS Fluent and Star CCM+ were considered for the simulation of the accelerating plates in this project. The latter was the one that was finally used. ANSYS Fluent was successfully used by Roohani and Skews [8] to simulate the accelerating aerofoils in 2D. They fixed the reference frame of the aerofoils while accelerating the flow field of the air around them. The user defined function that accelerated the far field while simultaneously accelerating the fluid inside boundaries using momentum and energy source terms was used [8].

Star CCM+ was preferred over ANSYS Fluent for the two reasons:

- Better presentation of the accelerating plate in the current experimental set-up.
- Simplicity of overset mesh in handling motion of rigid bodies (discussed in later sections).

Star CCM+ was preferred because its overset mesh has capability of making air stationary while the plate is accelerated exactly like it was the case in the experiment performed. This could not be achieved by Fluent as it does not have “facility for translational acceleration of the reference frame of an object” [8]. The overset mesh in Star CCM+ was found to be easier as the free stream Mach number around the domain was made zero and a field function for increasing the velocity of the plate at each time step in accordance with the acceleration used was assigned to the overset region that accelerated together with a plate inside a stationary background region [24].

In the experiment, the plate was at rest and in contact with a stationary magnet before accelerating. In overset mesh, the magnet was treated as a slip wall boundary. During acceleration, the distance between the magnet wall and the plate kept on increasing exactly like in the experiment since the reference frame of the plate could move inside a stationary air

or domain. If the method in reference [8] was to be used, the gap between magnet and plate would have to be constant since that method does not have the facility for translational acceleration of the reference frame of an object. The constant distance between a magnet and plate does not depict what happens in the experiment. The overset mesh in Star CCM+ was preferred because it displayed exactly what was happening in the experiment; the gap between a magnet and plate kept on increasing during the plate motion in the experiment.

The set-back of an overset mesh is that the domain would have to be very long if a translating body had to cover large displacements [25]. In that regard, the ANSYS Fluent method in [8] would be computationally cheaper as in that method, the body is fixed in a domain regardless of how long the physical displacement being simulated is. Because the plate being accelerated had to cover small displacement (less than 100mm) in the present project, the computational cost was not a concern. Therefore, the author went for the simpler field function that was created by simple equation of motion for bodies uniformly accelerated from rest (equation 1 section 4.1 page 18) in Star CCM+ overset meshing.

In the older releases of Star CCM+, the exact contact between plate wall and magnet boundaries would not be possible [26]. There has to be 2 to 4 cells between boundaries in order for overset mesh interface to work. The contact between the magnet and plate wall boundaries could not be achieved in that case. Refining the mesh to be as fine as possible between the magnet and plate boundary walls could only lead to those walls being as close as possible but not in contact. On top of the fact that the contact between the plate and magnet like in the current experimental set-up would not be possible, refining the mesh to make a plate to be as close as possible to the magnet would increase the computational cost. However, the simulation of contact between regions is no longer a problem in the latest releases of Star CCM+ (from 9.06 to the most recent 11.06). These latest releases have option of overset mesh zero gap interface that can handle contact of different regions without making a simulation to be computational expensive (overset mesh zero gap interface is revisited in chapter 4). Star CCM+ release 11.02 is used in this project.

2.4.2. Modelling turbulent flows

Turbulent flow is three dimensional and fluctuates with both space and time [27]. It is chaotic (full of both large and small eddies). Detailed solutions of Navier Stokes (N-S) equations (taking all eddies in turbulent flow into consideration) would be computationally expensive

and impractical to achieve [28]. Therefore, fluid dynamicists have resorted to time averaging (expressing instantaneous velocity and pressure fields as a sum of a mean value plus a fluctuating component [29]) leading to Reynolds Averaged Navier Stokes equations (RANS). Although the form of RANS is almost similar to N-S equations, the disadvantage of RANS is the tensor quantity called Reynolds Stress Tensor (RST) that arises during time averaging. There are different kinds of turbulence modelling used to solve this RST. They are eddy viscosity model (which can be divided into K-epsilon, K-omega and Spalart Allmaras) and Reynolds Stress Transport model [29].

Selecting a suitable turbulence model is very important in order to simulate boundary layers in turbulent flows just like selecting a suitable wall y^+ value in order to simulate a certain region of boundary layer. Regardless of the number of available turbulent models in fluid dynamics, simulating viscous turbulent flows accurately and efficiently is not easy. The reason is that turbulent transport processes are unique for a certain problem in hand and the same turbulent model in Star CCM+ might predict different results in ANSYS Fluent or other CFD codes [30].

The concept of wall y^+ “a dimensionless quantity which is the distance from the wall measured in terms of viscous lengths” [31] is used to handle the near wall behavior. The wall y^+ value can be divided into the following depending on the region of boundary layer that can be solved [32]:

- $Y^+ < 5$ for viscous sublayer region (velocity profile is assumed to be laminar and viscous stress dominates the wall shear)
- $5 < y^+ < 30$ for buffer region (both viscous and turbulent shear dominates) and
- $30 < y^+ < 300$ for fully turbulent portion or log-law region (turbulent shear predominates). Wall y^+ used will determine the size of the first cell near the wall and the boundary layer region corresponding to that y^+ can be simulated.

2.5. Experimental Flow Visualization

Vortex wakes can be so complex that it is highly advisable to analyse them by more than one method to avoid incorrect conclusions [33]. In this project, the analysis of flow around accelerating plates was achieved by applying the CFD method “Star CCM+ overset meshing” in parallel with experimental method “flow visualisation” for validation purposes. Flow visualisation techniques are of vital importance in flow around aerodynamic bodies as they

can act as a starting point for analysing complex flow parameters such as surface flow, flow separation and wakes [34].

The technique used in the current project falls under “flow visualisation by direct injection” discussed by Nelson and Babie [34]. The exact name for the method used here is called Laser Vapour Sheet (LVS) visualisation. In LVS, fine particles such as smoke are injected into the test area and a thin sheet of laser light is shone onto the test area [35]. The cross-section of the flow profile can be visualised from the reflection of light by the smoke particles on the sheet of light. If the sheet of light is placed at different planes on the object, an overview of 3D flow profile around such a body can be achieved. The reference [35] can be consulted for more information about LVS.

The important points for achieving a sufficient quality of the smoke for flow visualisation are [34]:

- The smoke particles should not disturb the flow
- Particles should be neutrally buoyant and have negligible inertial effects
- The particles should reflect light well
- Seeding media should be non-toxic and
- Smoke should be inexpensive.

Chapter 3: Experimental Method

3.1.Introduction

In order to validate the chosen CFD methodology for simulating flow around rapidly accelerating plates with particular interest in vortex shedding from their edges, experiments were performed. Initially, the aim was to do experiments on three different plates (circular, square and triangular). However, the cost of renting the laser limited the number of days for testing. Therefore, only circular plate which is axis-symmetric was tested experimentally. It was assumed that applying the CFD method that has been validated with an axis-symmetric or circular plate to asymmetric plates (square and triangular) would still give reliable results. However, the mesh and boundary conditions in simulating square and triangular plates had to be the same as the case of the circular plate that was validated experimentally.

In the experiment, the flow profile around 8 mm thick and 80 mm diameter circular plate was visualised using a Photron Fastcam SA5 high speed camera. The circular, triangular and square plates are shown on Figure 6 page 22. The name of the experimental method used is laser vapour sheet (LVS). The main system in the experiment was a rig designed by Wits School of Mechanical, Aeronautical and Industrial engineering shown in Figure 3 below.

3.2.Experimental Set-up

Figure 2 below shows the high level diagram of the experimental set-up that gives the quick overview of the experimental set-up:

- Plate accelerates uniformly from rest from $y = 0$ m to $y = 0.1$ m.
- Thin sheet of laser light is shone onto the test area around an accelerating plate.
- A high speed camera captures the flow profiles of the accelerating plate.
- Figure 3 shows the detailed diagram of the experimental set-up.

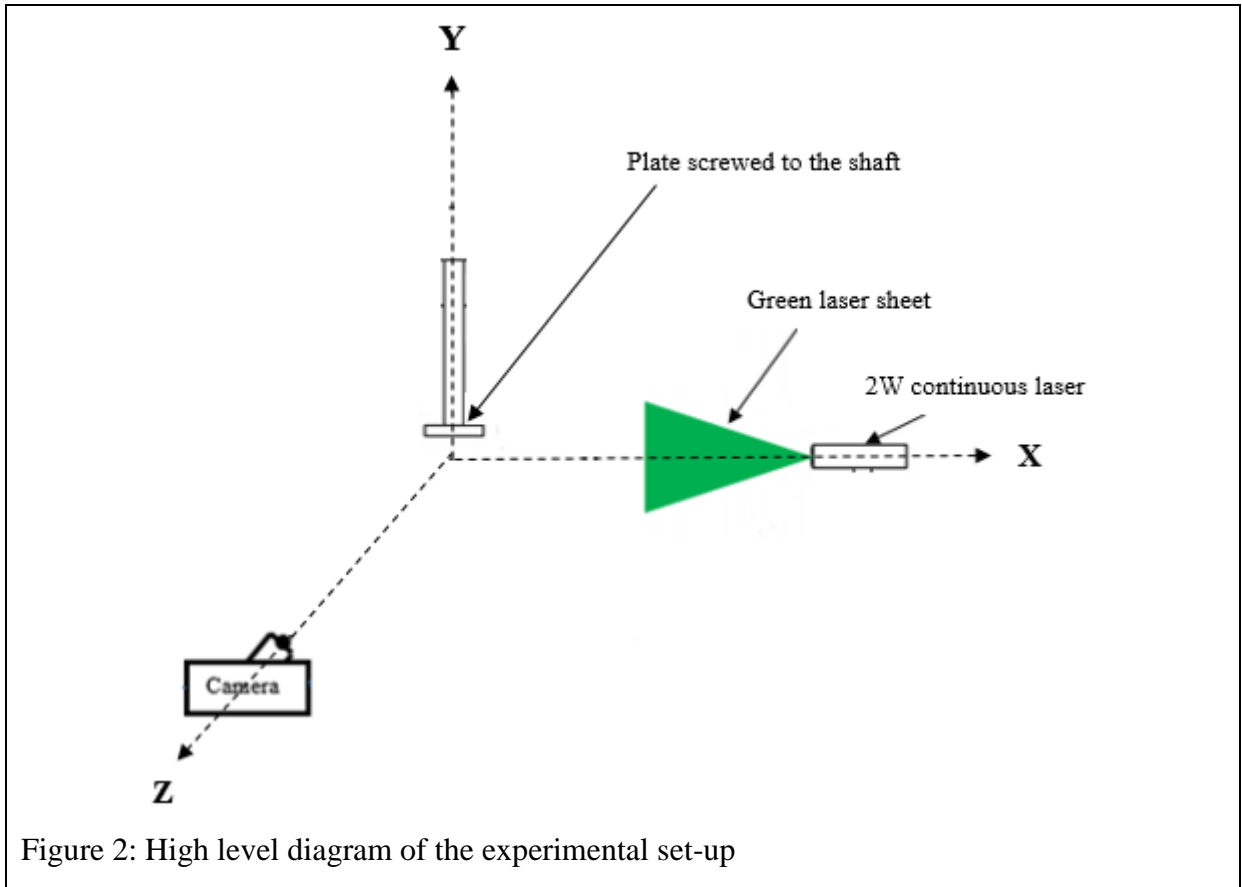


Figure 2: High level diagram of the experimental set-up

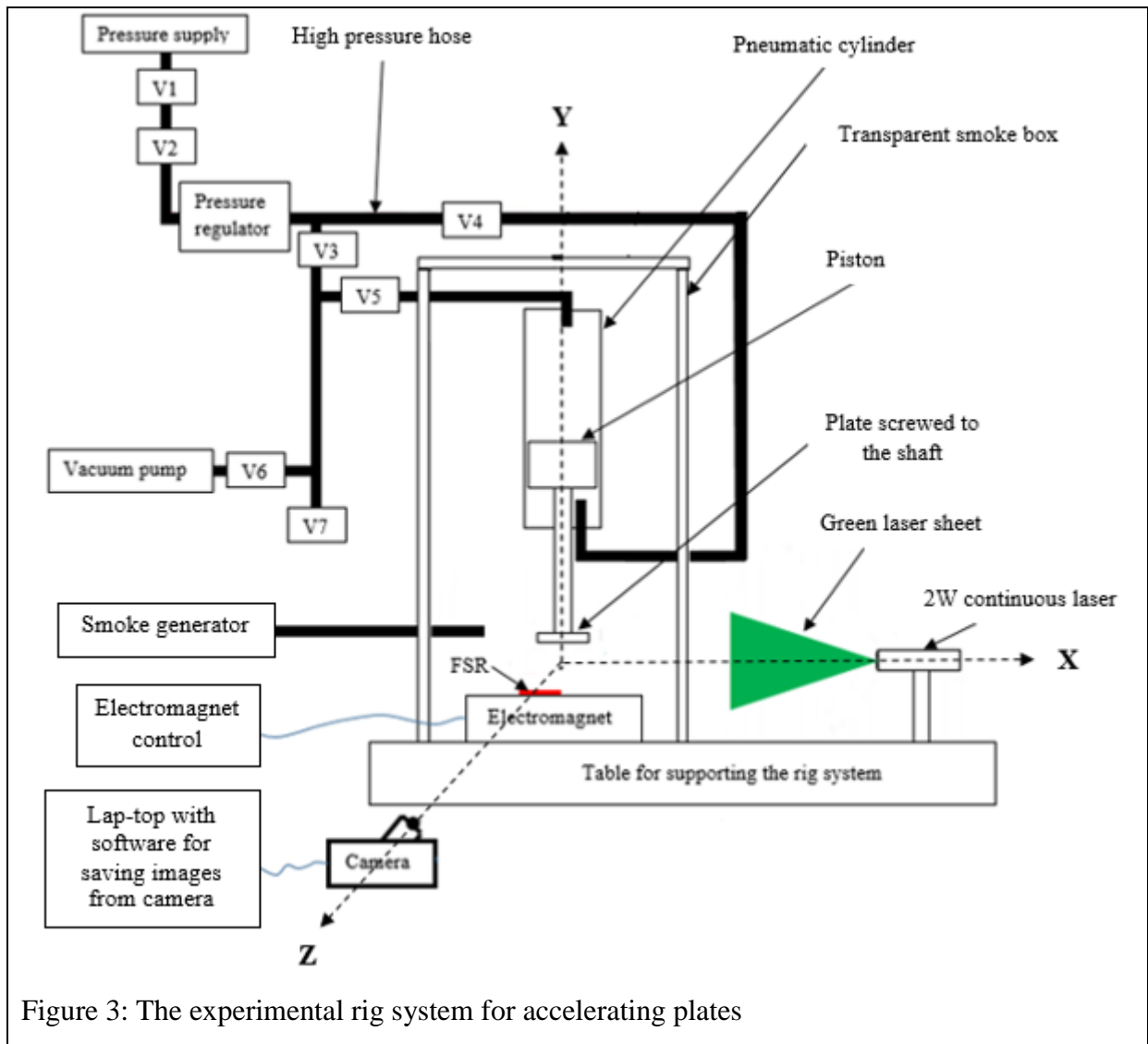


Figure 3: The experimental rig system for accelerating plates

3.3.List of Apparatus

Pressure supply: can supply up to 7 bar pressurized air from the compressor.

V1 to V7: Valves to control the flow of air in the system.

Pressure regulator: it sets the pressure in the system (pressure was set to 2bar throughout the experiment).

Vacuum pump: to set vacuum pressure in the system. Setting the pressure in the volume above the piston to vacuum increased a pressure differential between the upper and lower sides of the piston and consequently increasing acceleration.

Smoke generator (Safex Nebel Great F2004): supply the smoke inside the transparent smoke box.

Transparent smoke box: 800 x 800 x 600 transparent box to enclose the smoke produced by safex - nebelfluid normal power mix around the test area. It is transparent for the flow profile to be visible to the camera facing the test area.

Pneumatic cylinder and piston: the piston moves inside the cylinder to move the plate that is mounted to it by a shaft in upwards and downwards directions.

Electro-magnet: it holds the plate firmly when it is on and lets it go when it is off

Electro – magnet control: It turns on (activates) the electro-magnet when it is on and deactivates the magnet when it is off. It was playing a starter role in that it had to be turned off for the plate to accelerate.

Plate – 8mm thick and 80mm diameter circular plate screwed on a 22mm shaft. The experiment was done on this plate for validation purpose before simulating triangular and square plates. All three plates are shown on Figure 6 page 22.

2W – Laser

For producing a green laser sheet passing across the plate and providing the light for flow profile to be captured by a high speed camera. The laser light was shone on the xy plane (see Figure 3)

Force sensing resistor (FSR)

“A force sensing resistor (FSR) is a flat and flexible device that exhibits a decreasing electrical resistance with increasing force applied normal to its surface” [36]. The plate attracted by electromagnet pressed the FSR consequently reducing its resistance. When the acceleration motion began (the right time for triggering a high-speed camera to capture the images of the plate in motion), the plate lost contact with the FSR which was suddenly relieved from pressure hence sudden increase of resistance. The micro-controller of the triggering circuit was programmed to send +5V TTL signal to the high-speed camera through the BNC connector to trigger it when resistance from FSR increased.

The triggering circuit was basically the idea from Arduino just modified to suit the current application. Arduino is an open source that can be used with different sensors in many engineering applications (see reference [37] for Arduino information and appendix 2 for the circuit built for this project with its programming code).

High Speed Camera

The camera was placed on the yz-plane facing in a negative z-direction towards the area where the motion of a plate was taking place. That is the camera was facing in a direction perpendicular to the laser sheet that cuts the plate at xy-plane (see Figure 3).

3.4.Procedure for Capturing Images of Flow Profiles

1. Refer to Figure 3 above when reading this procedure.
2. All the valves (except V1 isolating pressure supply to the rest of the system) were opened to vent the system.
3. The pressure regulator was set to 2 bar.
4. The smoke was filled in the transparent box from a smoke generator.
5. The force sensing resistor (FSR) sensor was powered.
6. All the valves were closed and then V1, V2, V3 and V5 were opened consecutively in order to lower a plate towards an electro-magnet.

7. Electro-magnet was powered by electro-magnet control. Then the magnet held the plate firmly.
8. V1 was closed and all other valves were opened to vent the system.
9. V3 was closed and V1, V2 and V4 were opened to pressurise the bottom of the piston (the piston did not move as the magnet held the plate). The magnetic force was greater than the pressurized force trying to accelerate the plate.
10. V7 was closed, V5 and V6 were opened and the vacuum pump was turned on to create vacuum on the top of the piston. This increased a pressure differential between the top and bottom sides of the piston.
11. The laser was powered and the laser sheet passed across the plate at xy-plane.
12. The high-speed camera facing the region around plate (facing in a negative z-direction on Figure 3 above) was powered.
13. The electro-magnet was turned off from its control and the plate accelerated in the positive y-direction and the FSR triggered the camera to capture many images during the motion of the plate. The number of images captured depended on the frame rate set on the camera; frame rate was set to 250. The photos were saved in a lap-top.
14. V1 was closed and vacuum pump turned off. Then all the valves except V1 were opened to vent the system and the process was repeated until the clear flow profiles of the vortices around the accelerating plate were captured.

3.5.Procedure for Determining the Experimental Acceleration

The acceleration at which the flow profiles of the accelerating plate were captured had to be experimentally determined so that the same acceleration could be used in the simulation for experimental and CFD results comparison under a common acceleration. In order to determine the experimental plate acceleration, the graph of plate displacement versus time of the accelerating plate was plotted and the 2th order degree polynomial equation of that graph was differentiated twice to get acceleration. The experimental acceleration was obtained to be 13g. The procedure for determining displacement versus time for the accelerating plate is discussed chapter 5.

Chapter 4: CFD method used

This chapter covers the CFD methodology used. Experiments were done on the circular plate only; the CFD method discussed below was firstly applied to the circular plate and validated with the experimental results of the plate before simulating asymmetric plates (square and triangular). All plates are shown on Figure 6 page 22.

4.1. Problem Description

The simulation is of the plate accelerating uniformly from rest in a positive y-direction (from $y = 0$ m to $y = 0.1$ m) covering a total displacement of 0.1 m in stationary air. Figure 4 below shows how the domain for simulation was cut from the main experimental setup in Figure 3 page 14. The acceleration value determined experimentally (13g) was the one used for simulations so that experimental and CFD results could be compared under the same conditions. The velocity of the plate at each time step is represented by equation (1):

$$V_p(t) = a_p t \quad (1)$$

Where time is $0 \leq t \leq 0.04$ s and a_p is 13g or 127 m/s² (plate acceleration determined experimentally). The upper limit of time ($t = 0.04$ s) was selected in such a way that the total displacement given by equation 2 below $S(0.04) = 0.1$ m (0.1 m is the total actual displacement that could be reached experimentally by the rig used).

$$S(t) = 0.5a_p t^2 \quad (2)$$

The instantaneous Reynolds number at each time step $Re(t)$ was determined by equation (3):

$$Re(t) = \frac{\rho V_p(t) D}{\mu} \quad (3)$$

Where ρ is the density of air (1.225 kg/m³), $V_p(t)$ is the plate velocity in m/s at time t , D is diameter of the plate (0.08 m in the case of circular plate) and μ is the dynamic viscosity of air (1.81x10⁻⁵ kg/(m.s)).

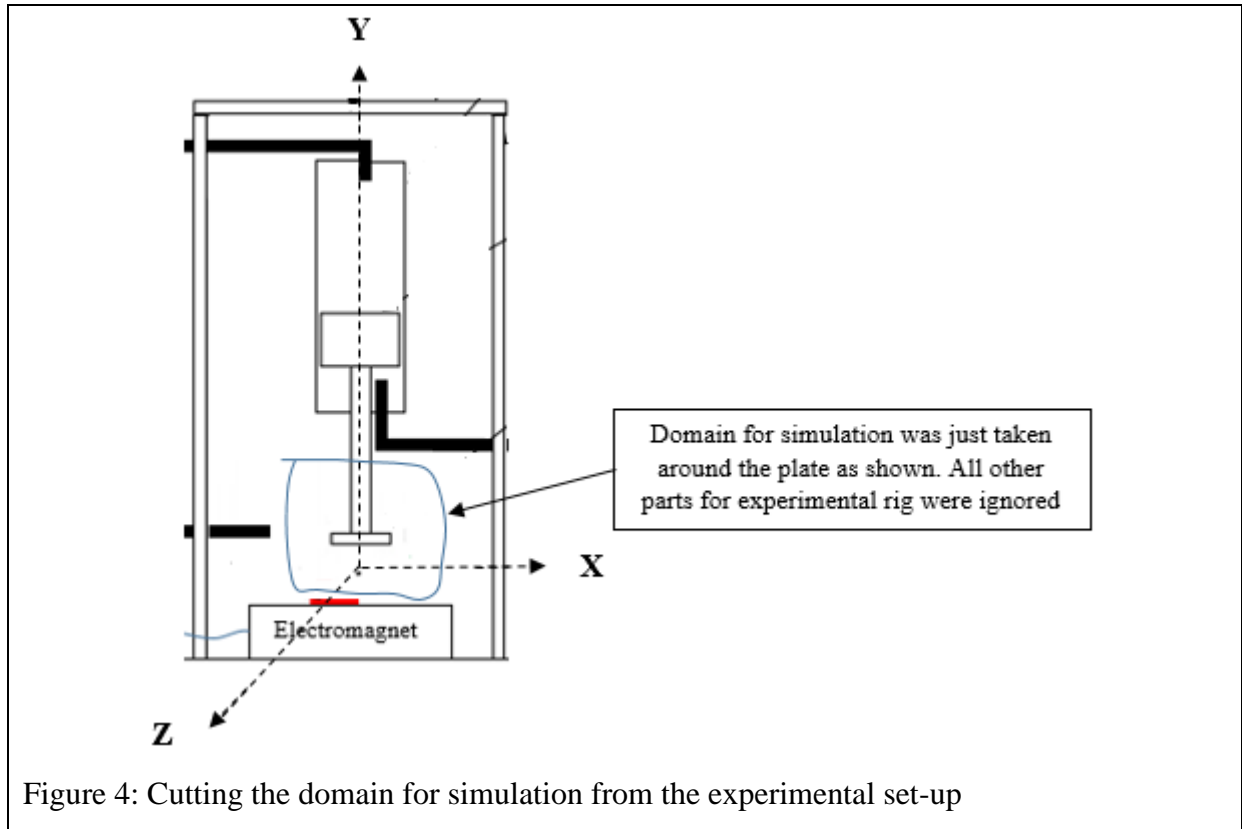


Figure 4: Cutting the domain for simulation from the experimental set-up

The Table 1 below summarises some constants important in the simulation of accelerating plate.

Table 1: Some constants of accelerating plate at final time step

Total plate displacement S (m)	Acceleration a (g)	Time taken by plate in motion $t = \sqrt{\frac{2S}{a}}$ (s)	Final velocity of the plate $V = at$ (m/s)	Final Reynolds number Re
0.1	13	0.04	5	27505

The equation for plate velocity (Equation 1 above) was used as a field function in Star CCM+ for ensuring that the velocity of a plate increased with increasing time step. Time of 0.04 s was used as a stopping criteria ensuring that the simulation stops when a plate has covered the total displacement of 0.1 m (which is the total displacement covered by each plate in the experiment).

4.2. Geometry and Boundary Conditions

Figure 5 below shows the 2D representation of the geometry that was created (z-axis not shown). The origin was chosen to coincide with the centroid of the plate before the

simulation was run. The plate accelerates uniformly from rest from origin to $y = 0.1$ m with uniform acceleration of 127 m/s^2 . The coordinate system for simulation in Figure 5 below coincides with the coordinate system for the experiment in Figure 3 page 14.

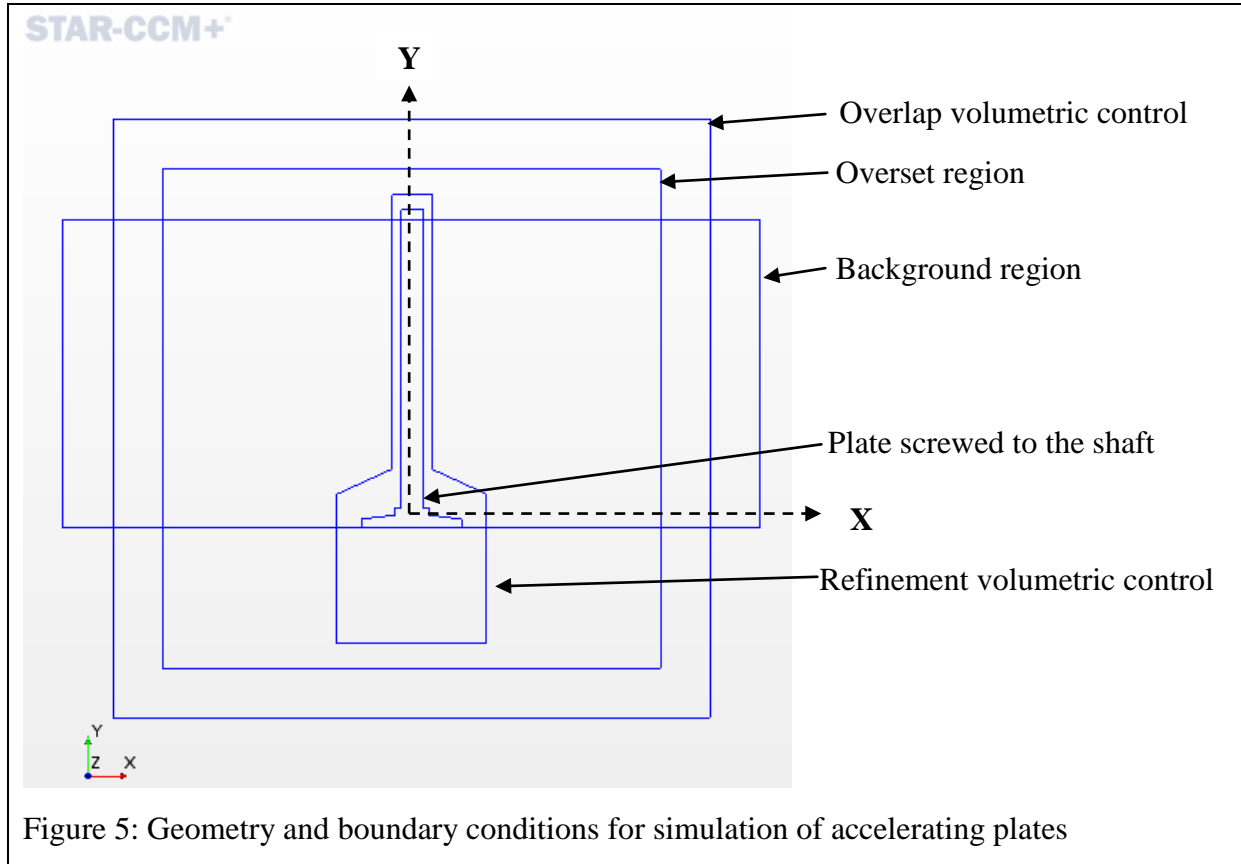


Figure 5: Geometry and boundary conditions for simulation of accelerating plates

Background Region

It represents the domain of the simulation. The physics motion specification of this region was set to stationary so that the region does not move during the simulation. When the simulation is initialised, everything that is outside this region breaks up as shown on the mesh on Figure 7 page 25.

The horizontal part of the background region that is in contact with the plate before the simulation starts (Figure 5 above) represents the magnet in the experiment. This magnet was allocated to slip wall boundary condition to avoid resolving the boundary layer on this wall. Apart from this magnetic slip wall, all other sides around the background region were set to freestream boundary condition. In order to represent the stationary air, the Mach number on this freestream boundary was set to zero.

Overset Region

This region contains the plate screwed to the shaft and was allocated to an overset mesh boundary condition. The physics specification of this region was set to translation. This region translates in a positive y-direction according to the field function built by Equation 1 (page 18) in Star CCM+. The field function is the equation of motion for a plate uniformly accelerated from rest. It updates the overset region and plate velocities at each time step according to the acceleration of 127 m/s^2 used.

Overlap Volumetric Control

In order for the overset region to move inside a stationary background region, the volumetric control is required to couple the two regions. This volumetric control also ensures that the background and overset meshes have the same cell-size where they interact.

Refinement Volumetric Control

Referring to Figure 5 above, one way of avoiding too much computational cost was to make overset region to be far away from the plate so that a course mesh could be used. The errors due to coarse mesh were not that significant on the plate as the boundaries of the overset region were far enough from the plate. However, the volumetric control for refinement was drawn around the plate as the refinement was still needed to capture flow features around the plate or area of interest. The mesh on this volumetric control was refined to accurately handle flow features such as separation, boundary layer and vortices. This refined mesh also accelerated with the overset region and plate according to field function built by Equation 1 in page 18.

Plate screwed to the shaft

Figure 6 below shows three 8mm thick plates of the same cross-sectional areas (108mm length equilateral triangular, 71mm length square and 80mm diameter circular) that were simulated. They were all screwed to a 22 mm diameter shaft. The mesh, boundary conditions and physics were identical for all plates during the simulation. The boundary condition of each plate was set to no slip wall.

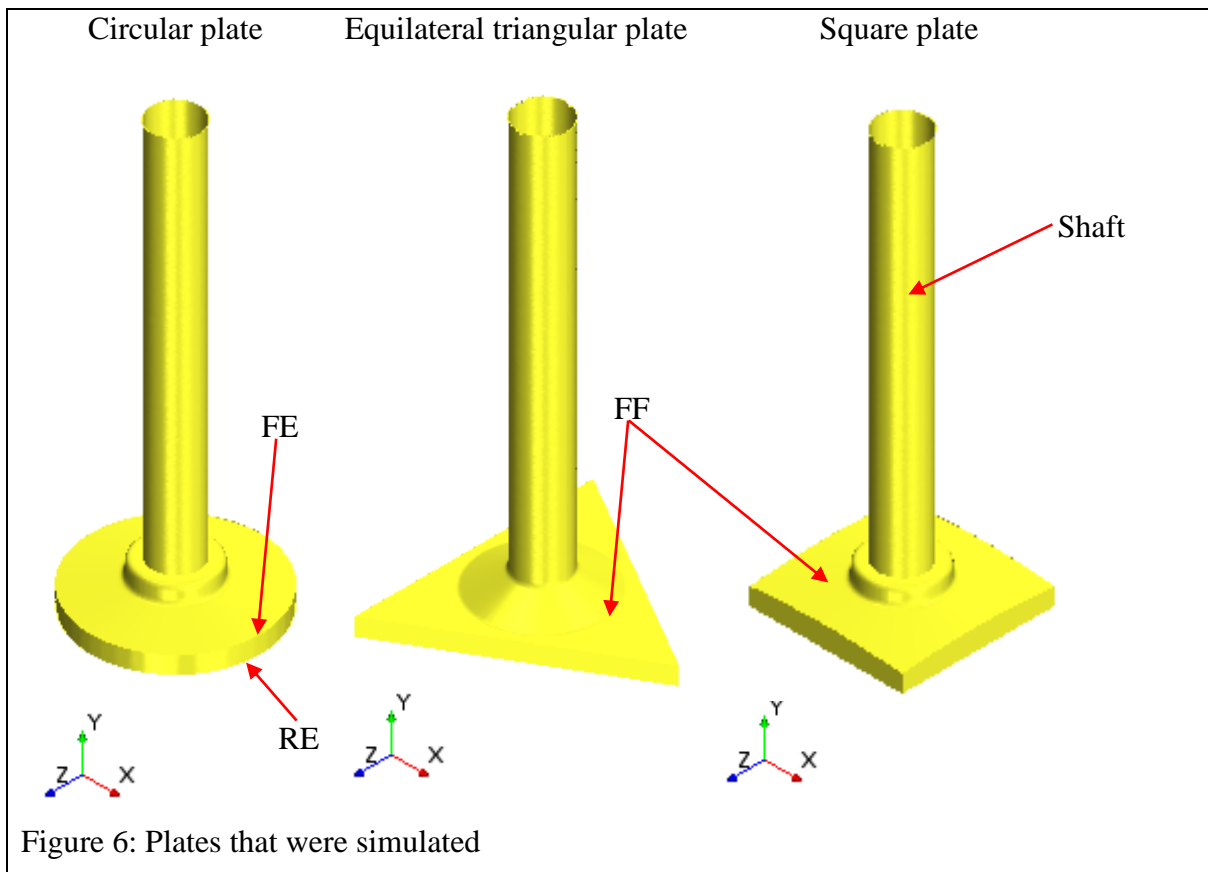


Figure 6: Plates that were simulated

From Figure 6 above:

- FF is a front face of the plate; the face on the side with a shaft
- RF (not labelled) is a rear face; the face on the side without shaft
- FE is a front edge; the edge of the plate on the side with a shaft.
- RE is a rear edge on the plate; the edge on the side without a shaft

The front edge (FE) would be used frequently as the front edges become the edges of separation where fluid particles displaced by from front face (FF) separate at. The side of a shaft is referred as a front side because the motion of a plate is in a positive y-direction.

4.3.Meshing

The method of simulation used is overset (chimera) mesh from Star CCM+ commercial CFD package. The overset mesh was used as it does not require mesh modification after generation of the initial mesh hence being able to handle motion better than other standard meshing techniques [24]. The overset region which contains the plate with its shaft was created and

could accelerate inside the stationary background region. The 2D mesh (z-coordinate not shown) is shown on Figure 7 page 25.

Like many CFD software, Star CCM+ uses finite volume method to discretise the domain into small grids where pressure and velocity fields are computed. The overset region together with a plate accelerates inside a stationary background region. The background and overset regions are coupled together by volumetric control “overlap for refinement” which also ensures the same cell size between the overset boundary/interface and the Background. Volumetric control for refinement was created in order to refine around a plate and its wake region (see Figure 5 page 20).

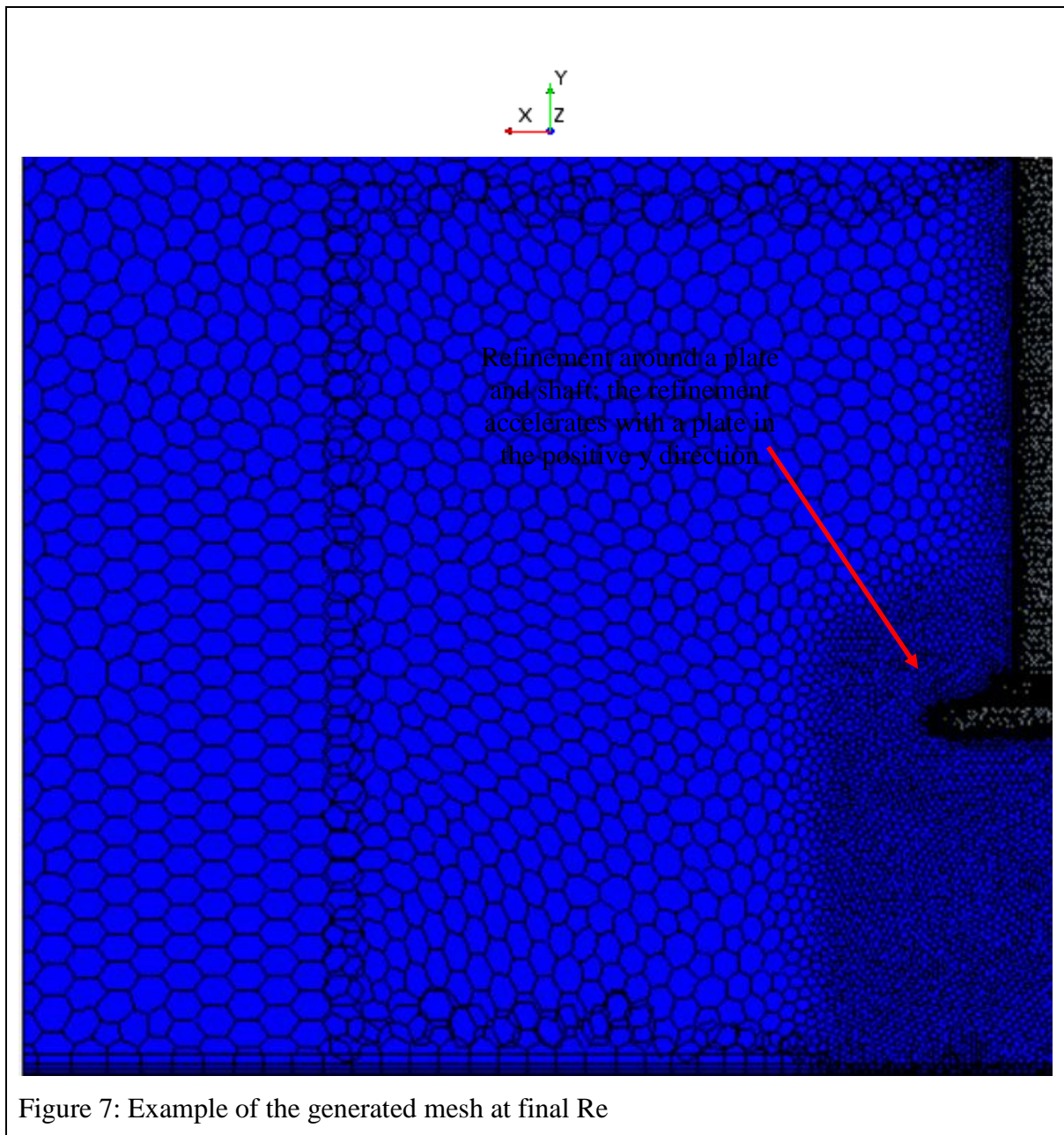
The volume mesh was chosen based on the computational cost and accuracy in handling the current problem which has a high level of separation due to sharp edges of the plate and overall orientation of the plate to its direction of motion. Polyhedral and trimmer meshers were both considered. The polyhedral mesh is more accurate and converges faster when compared to tetrahedral mesh. Although trimmed mesh require less memory than polyhedral mesh, it does not provide conformal mesh at the interface between separate regions [29].

Polyhedral mesh is also good for flow with swirl/ recirculation [29] hence being a good choice for capturing vortex shedding. Polyhedral cells having more faces as compared to either tetrahedral or hexahedral, the chances of flow direction being almost if not orthogonal to the polyhedral mesh face are higher regardless of how random the flow directions can be. The more neighbors in polyhedral mesh also allows for a better gradient approximation, especially near boundaries and corners [38]. Prism layer mesher was activated in order to accurately simulate the turbulence near the wall.

Table 2: Mesh information

Parameter	Description	Value
Volume mesh used	Polyhedral	
Base size		0.1 m
Number of prism layers		5
Prism layer thickness	Relative size	7.5 %
Surface size	Relative minimum	10 %
	Target	10 %
Volumetric control	Overlap relative size	10 %
	Refinement relative size	2.5 %
Plate + shaft boundary	Number of prism layers	5
	Prism layer thickness	1 %
	Relative size	0.5 %
	Relative minimum	1.5 %
Prism layer mesher	Gap fill	49 %
	Minimum thickness	0.01 %
	Boundary march angle	85

The resulting mesh is shown below:



Comments about the mesh

In the mesh in Figure 7 above, the overset region was created far from the plate (area of interest). The reason was to get away with a coarse mesh as 3D simulation is computationally expensive. When the overset region is far from the plate, the errors caused by a course mesh does not have a significant effect on the plate being investigated [39]. The refinement was done around the plate and shaft to capture important flow features around them.

4.4. Physics of uniformly accelerated plate from rest

The following physics models were selected and the models that were automatically selected by Star CCM+ were found to be compatible with the current simulation:

- Coupled flow
- Gas
- Ideal gas
- Implicit unsteady
- Turbulent
- K-Epsilon Turbulence
- Three dimensional, Coupled energy, gradients, K-Epsilon Two-layer, Two-layer All y+ wall treatment, Reynolds-Averaged Navier-Stokes (automatically selected by Star CCM+)

It has already been introduced that the plate with its shaft was accelerating together with the overset region inside a stationary background region with acceleration that was determined experimentally (13g or 127 m/s²). The communication between the overset and background regions was ensured by creating an “overset mesh zero gap” interface with close proximity between the two regions. Overset mesh zero gap interface is only found in the latest releases of Star CCM+ (9.06 release upwards) [26]. This type of interface creates a zero gap boundary where two or more regions contact or come very close to each other [24]. The cells on both regions at that contact or small gap deactivated and reactivated again once the gap reopens [24]. This advancement is new in Star CCM+ and it enables the overset region to extend beyond the boundaries of the domain as applied in in the current simulation whereby the part of a shaft is continually disappearing outside the domain during the plate acceleration.

The motion specification of the overset region was set to “translation” to ensure that it was accelerating inside a stationary background region that was left with default “stationary” motion specification. The overset motion specification was automatically linked to the translation field function “[0.0, 127*\$Time, 0.0]” created under motion tools in Star CCM+. The field function ensures that the velocity in the y-direction increases per time step which is set under solvers. This field function is nothing but the equation of motion for bodies accelerating uniformly from rest (Equation 1 page 18). The suitable time step was estimated by Equation 4 below [39]:

$$\text{Courant number} = V_{pf} \frac{\Delta t}{\Delta x} \quad (4)$$

Where a Courant number of 1 was assumed, final velocity V_{pf} was from Table 1 page 19 (5m/s) and Δx was taken as half of the smallest cell size in the overlap region since a second order temporal discretisation scheme was used [39]. The Mach number from freestream boundary around the background region was set to zero to ensure that the plate was accelerating in a stationary air like in the experiment. The stopping criteria was set to 0.04 s which is the time for a plate accelerating from rest at 13g or 127 m/s² to reach displacement of 0.1 m as in the experiment.

Referring to Table 1 on page 19, the displacement of 0.1 m for plate accelerating uniformly from rest at 13g or 127 m/s² acceleration limits the final velocity to around 5 m/s (Mach number far less than 0.3). Therefore, a segregated solver which is suitable for “incompressible or weakly compressible flows” [40] could still work fine for those small Mach numbers. However, coupled implicit solvers that solve linearised equations of momentum and continuity equations simultaneously (unlike the segregated solver that solves them independently) [41] was not only used for generally being accurate in compressible flows [40] but also for having a better convergence in swirling flows where coupling between the radial and tangential momentum equations is strong [41].

The flow of accelerating flat plate with direction of motion perpendicular to its flat surfaces is very unsteady with time and sheds vortices on the plate wake. Therefore, turbulent modelling was activated in order to generally cater for the chaotic behavior of the flow in the current project. Reynolds Stress Transport model is computationally expensive and usually advised when the CFD engineer has acquired a lot of experience in CFD [29]. Therefore, Reynolds stress tensor was solved by selecting a suitable turbulence model from the eddy viscosity model group. K-epsilon model was selected over Spalart-Allmaras and K-Omega models due to being better in handling flows with “complex recirculation and having a good compromise between robustness, computational cost and accuracy” [29].

Davis, Rinehimer and Uddin [38] found the $k - \epsilon$ turbulence model to produce results closest to the experiment when comparing how different models could predict visualisation of

separated flows over a wall mounted circular cylinder at constant Reynolds number ($Re = 12\,000$). Reliasable $k - \epsilon$ was superior in displaying complex flow structures such as re-circulation zones, counter-rotating and alternatively shedding vortices and saddle region that reflects some shear layers away from it. Therefore, it was believed that $k - \epsilon$ would perform well even in the current problem whereby sharp-edged bluff bodies are accelerating in air.

Chapter 5: Results and discussion

5.1. Calculation of experimental acceleration of a circular plate

In Chapter 3, it was stated that the acceleration was determined by finding the second derivative of displacement versus time graph. This section goes into detail on how acceleration was obtained. The number of images that can be captured by a high speed camera depends on the frame rate set on it. A frame rate of 250 was used in the current experiment due to having a good compromise between the brightness and number of images that could display development of vortices around the accelerating plate.

When a frame rate of 250 was set on a high speed camera, the plate took 0.04 s to reach the final displacement of 0.1 m and 10 images were captured. The displacement of a plate from the initial position was measured with a ruler on each image (see Figure 8 below). These displacements were not the real ones as their magnitudes depended on the scale of the paper that the photos were printed on. The actual displacement (S) was obtained by multiplying the displacements on the printed images (S_{image}) with a ratio of the actual shaft diameter as measured from the experiment (D_{actual}) and the shaft diameter as measured on the images (D_{image}). The high speed camera printed the time elapsed when each image was captured on each image (T_{image}) which is equal to the actual time T in the experiment. The displacement versus time graph was recorded. The equation of the graph (which is a 2nd order polynomial function) was differentiated twice to get acceleration.

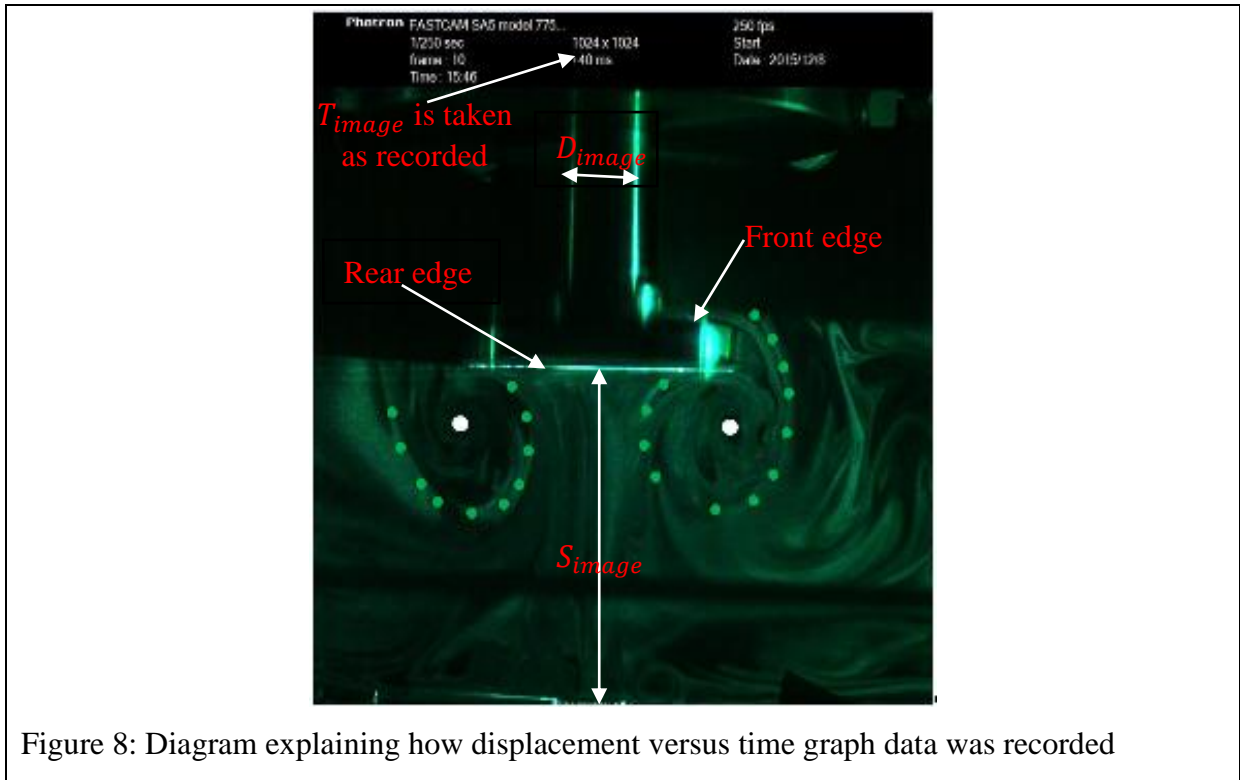


Figure 8: Diagram explaining how displacement versus time graph data was recorded

Converting the displacement (S_{image}) on the image to real displacement in the experiment (S) was done by equation 5 below:

$$S = S_{image} \times \frac{D_{actual}}{D_{image}} \quad (5)$$

Where S is the real displacement in the experiment, S_{image} is the displacement as measured from the image, D_{image} is the shaft diameter as measured from the image and D_{actual} is the actual diameter as measured in the experiment.

The graph of displacement versus time for accelerating circular plate is shown on Figure 9 below and the data in appendix 3 in Table 11 page 80.

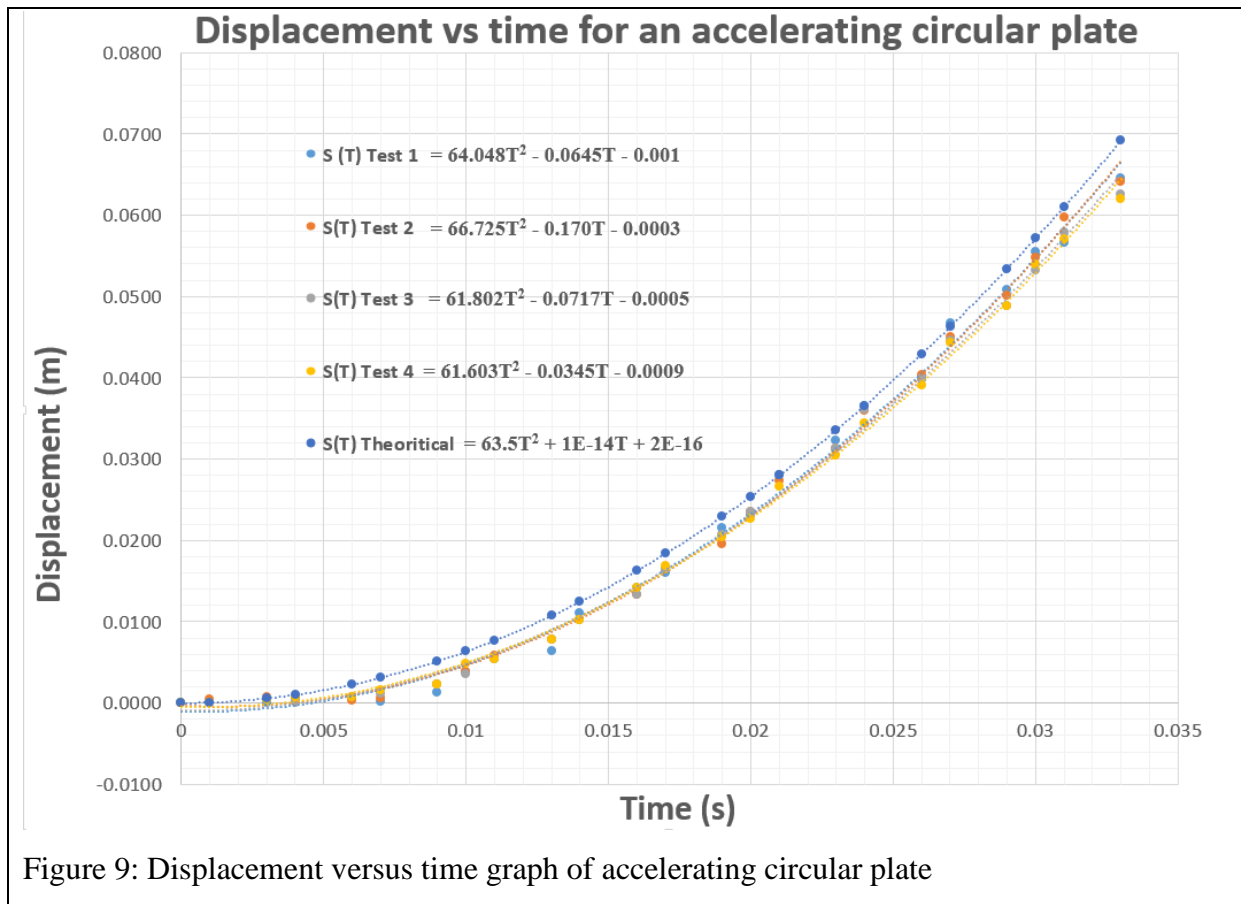


Figure 9: Displacement versus time graph of accelerating circular plate

Table 3: Estimation of circular plate acceleration

Test	Function $S(T)$ (m)	$\frac{d^2S}{dt^2} = \text{Acceleration (ms}^{-2}\text{)}$
1	$S(T) = 64.048T^2 - 0.0645T - 0.001$	128
2	$S(T) = 66.725T^2 - 0.170T - 0.0003$	133.4
3	$S(T) = 64.048T^2 - 0.0645T - 0.001$	128
4	$S(T) = 61.603T^2 - 0.0345T - 0.0009$	123.2
Theoretical	$S(T) = 0.5a_pT^2$	127
The experimental acceleration a_p was estimated to be $127 \text{ m/s}^2 = 13g$		

The experimental acceleration was estimated to be 127 m/s^2 or $13g$. This acceleration was estimated by differentiating a 2nd order polynomial function of the graph of experimental displacement of the plate versus time graph twice. The accuracy of the estimated acceleration was checked in two ways:

- Substituting the calculated acceleration of 127 m/s^2 into the equation of motion for displacement of bodies uniformly accelerated from rest (equation 2 on page 18). For $a_p = 127 \text{ m/s}^2$:

$$S(t) = 0.5a_p t^2 = 0.5(127)t^2, \quad \text{where } 0 \leq t \leq 0.04s$$

The resulting theoretical equation $S(t) = 0.5(127)t^2$ was used to obtain the theoretical displacements. Theoretical displacement versus time graph was plotted on the same graph with experimentally measured displacements (see Figure 9).

- Using the final time obtained in the experiment ($t = 0.04s$) with the estimated theoretical acceleration of 127 m/s^2 in the same equation 2 and calculate the displacement. For $t = 0.04 \text{ s}$:

$$S(t) = S(0.04) = 0.5(127)(0.04)^2 = 0.1016m$$

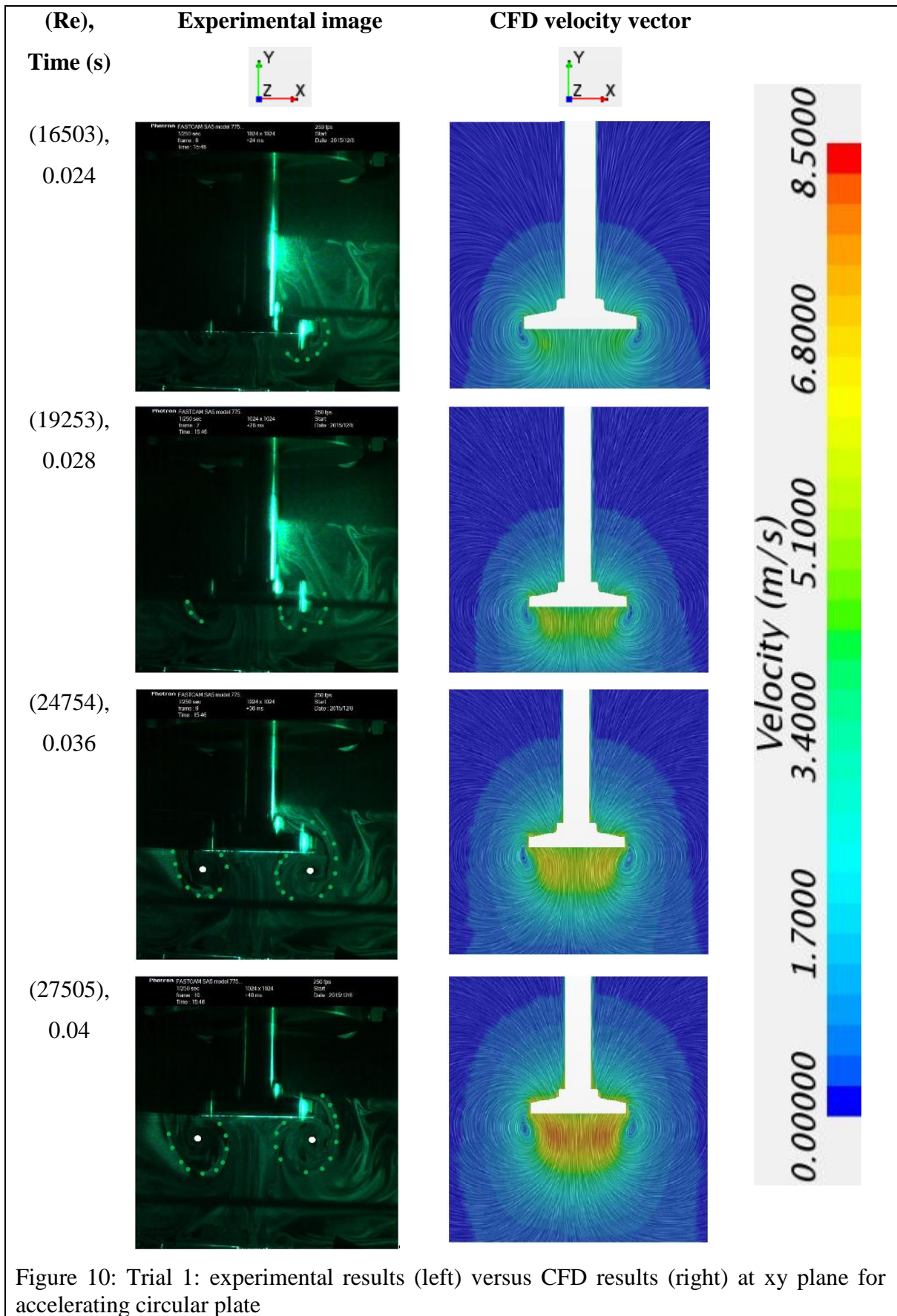
The estimation of acceleration was found to be accurate because when that acceleration of 127 m/s^2 was used in the displacement equation of motion of a body accelerating uniformly from rest (Equation 2), the theoretical displacement versus time graph obtained was consistent with the experimental data (see Figure 9 above that the theoretical graph is a best-fit line for experimental graphs). Secondly, when the estimated acceleration is substituted in equation of motion for bodies uniformly accelerated from rest, the displacement that is close to the displacement of $0.1m$ (reached by accelerating plate in the experiment) is obtained with a small percentage error of 1.6% $\left(\frac{0.1016-0.1}{0.1} \times 100\% = 1.6\%\right)$.

5.2.Results of vortices shed by accelerating circular Plate

5.2.1. Validation of results for accelerating circular plate

Before discussing validation of the results, it must be noted that the green and white dots on the experimental images on Figure 10 to Figure 13 were inserted manually in an attempt to trace a certain shear layer and vortex core respectively.

The experimental results of the accelerating circular plate on Figure 10 to Figure 13 below have been obtained using the laser vapour sheet method. There are many different ways at which vortices can be displayed in CFD. However, for the sake of this validation, velocity vector scenes in line integral convolution mode were found to be more of the representation of how shear layers or air particles move around the plate in the experiment. So the CFD vector scene is compared with the experimental results for validation purposes. But after validation, the iso-surfaces of lambda 2 criterion method of vortex identification based on velocity gradient tensor will be used as it focuses more on extracting the vortices in the domain.



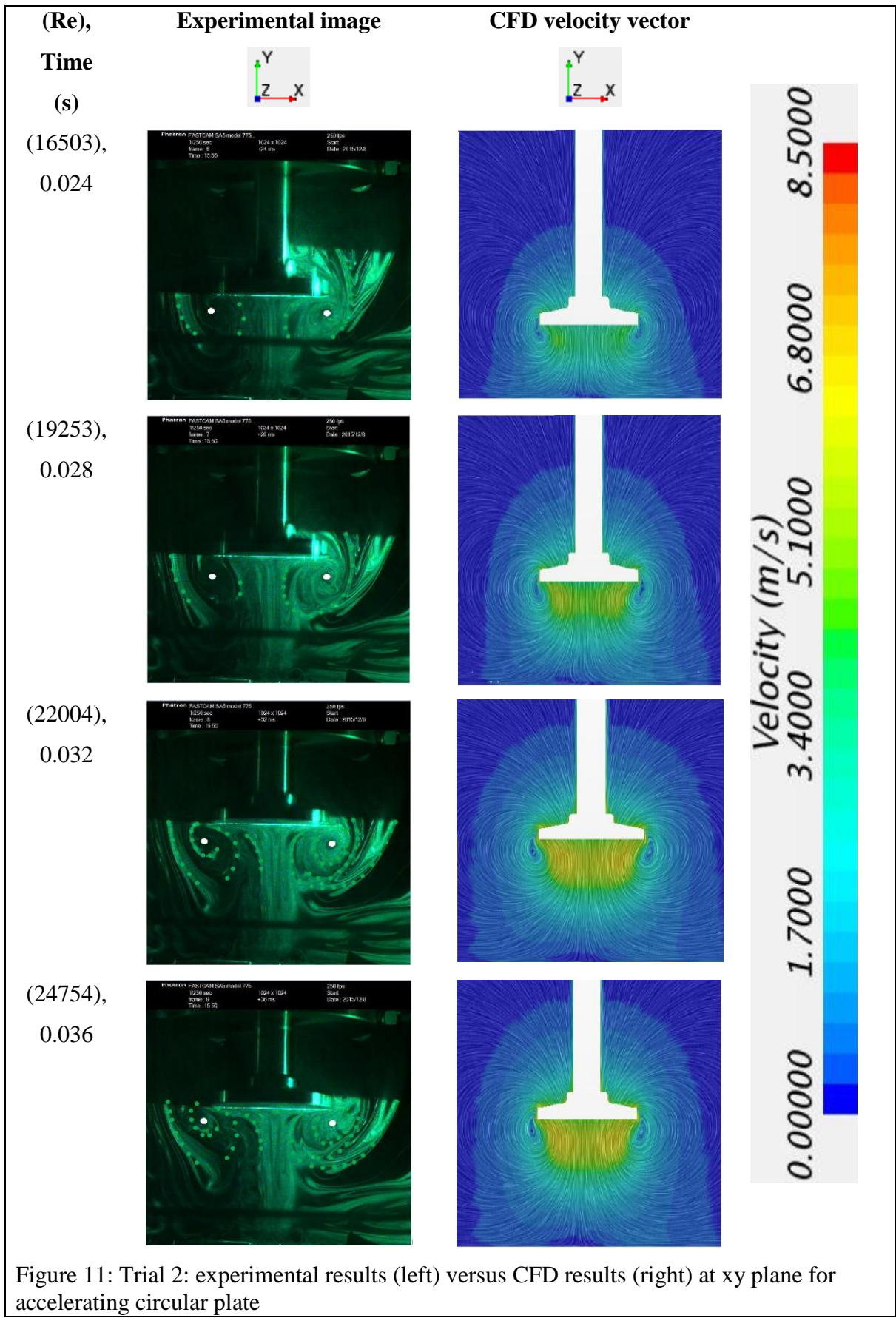


Figure 11: Trial 2: experimental results (left) versus CFD results (right) at xy plane for accelerating circular plate

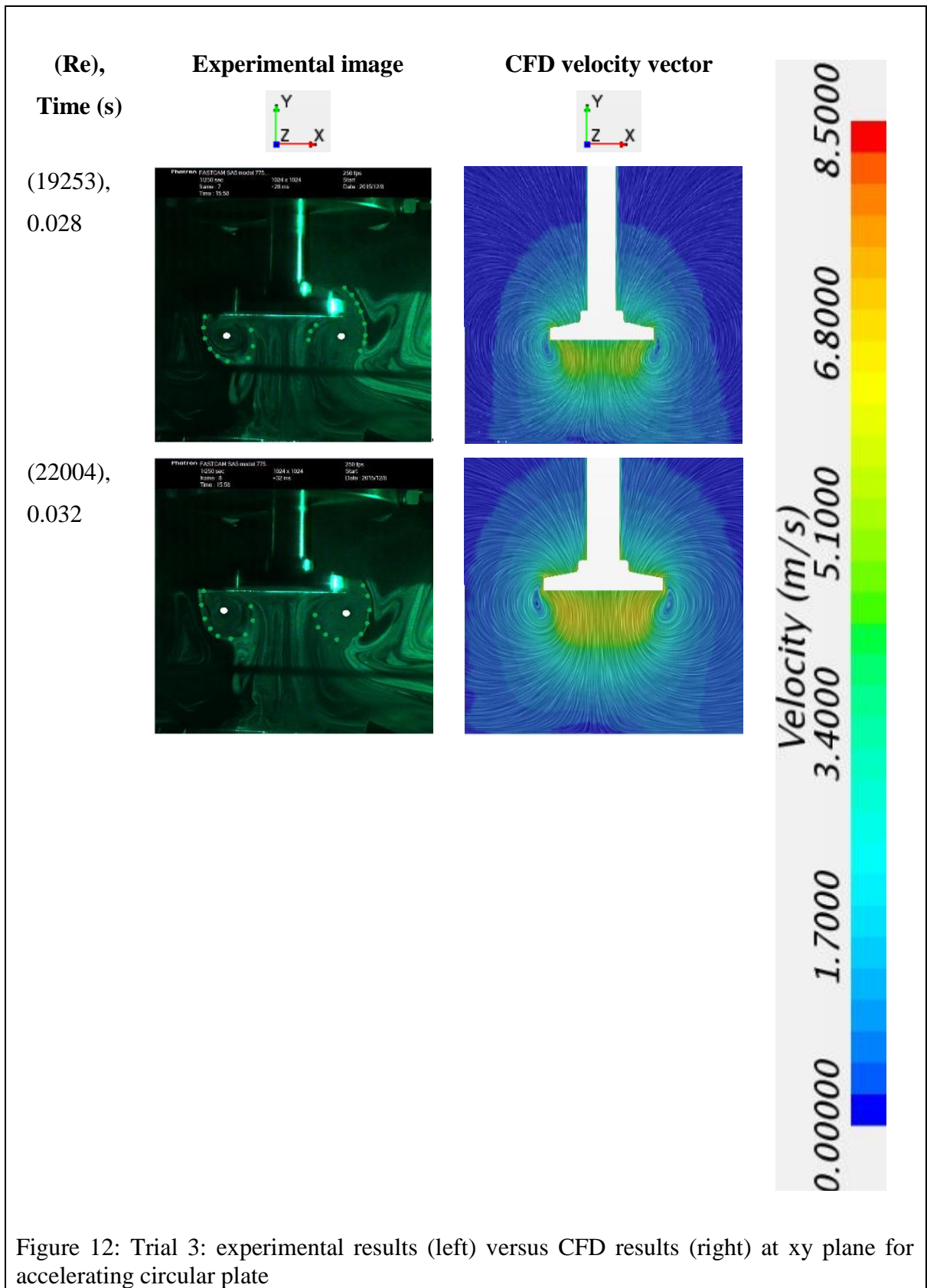
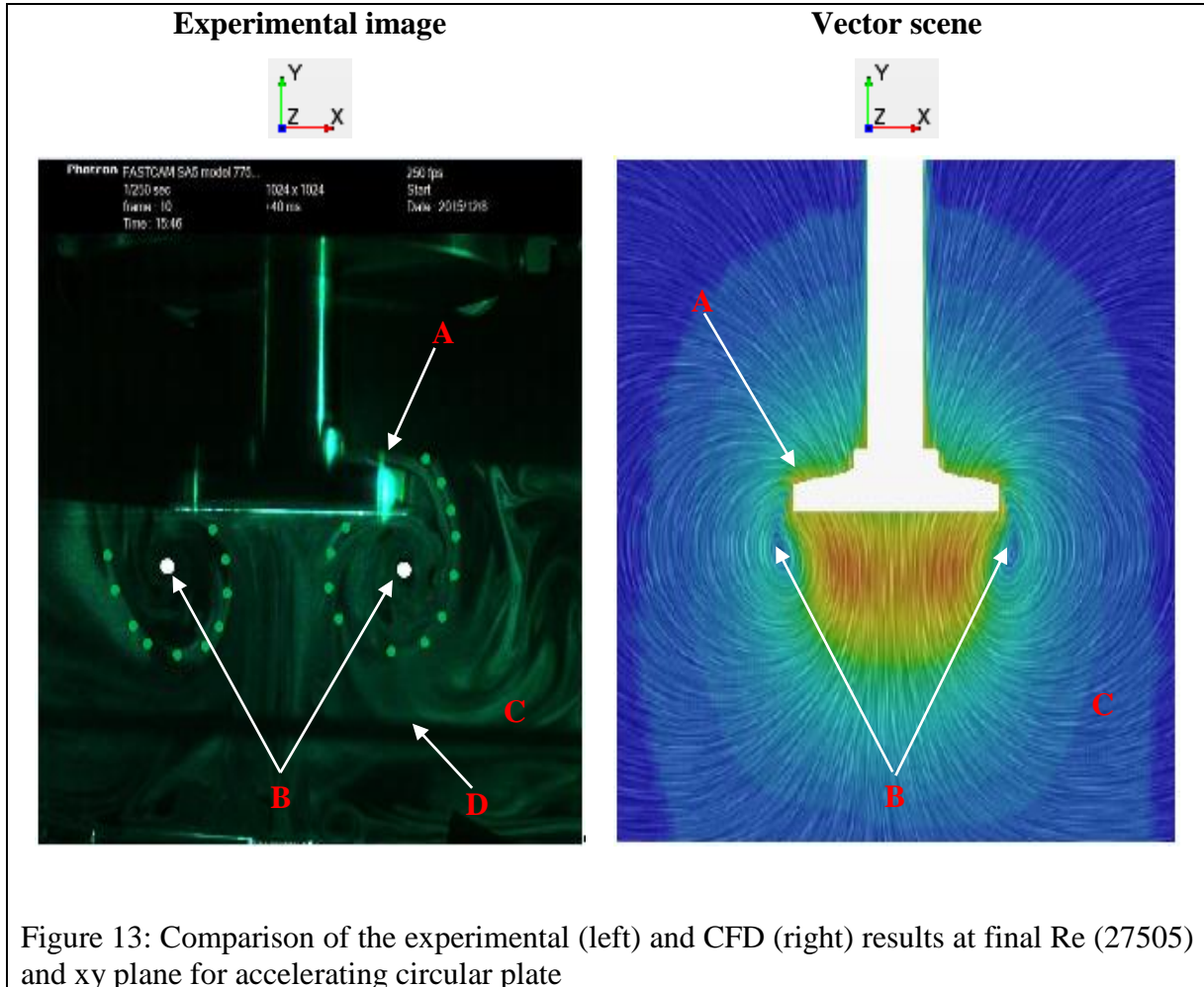


Figure 12: Trial 3: experimental results (left) versus CFD results (right) at xy plane for accelerating circular plate

At final Re, the flow features are well-developed. Therefore, the terminology or flow features that would be used in this results discussion are introduced by making use of the results from the final Re (27505) from Figure 10.



From Figure 13 above:

- A = Main shear layer separating at the front edge of the plate and catapulted outwards away from plate axis, rolling into what appears to be two counter-rotating primary vortices around the vortex core B at wake of the plate. The vortex on the left side of the plate axis is the mirror image of the one on the right with a mirror line y-axis. The separation of shear layer A is displayed better by the experimental image. **Note** that in 2D and in Figure 13 above, the primary vortex appears to be two counter-rotating vortices on both sides of the y-axis. In actual fact and in 3D, primary vortex is an axis-symmetric ring that results when 2D representation of vortex in Figure 13 is

revolved around y-axis through 360°. The 3D representation of primary vortex ring at various Reynolds numbers is shown in Figure 16, page 43.

- B = Vortex core of a primary vortex. **Note** that in 2D and in Figure 13 above, the vortex core appears to be the two dots on both sides of the y-axis. In actual fact and in 3D, vortex core is a continuous circle that results when 2D representation of vortex in Figure 13 is revolved around y-axis through 360°. The 3D representation of vortex core at various Reynolds numbers is shown on Figure 14 to Figure 16, page 40 to 43.
- C = Any air particle or shear layer at any point rolls around the main shear layer A with a radius of curvature that depends on how far that air particle is from the vortex core B. As the distance from the air particle to the vortex core increases, the radius of curvature that the air particle rolls around the vortex core also increases. This point is well-displayed by CFD; the vector scene shows the curvature at which all the fluid particles in the domain are following around the vortex core.
- D (appear as a dark line in the experimental results) is a shadow of something that might be in front of the laser; it is not part of the results.

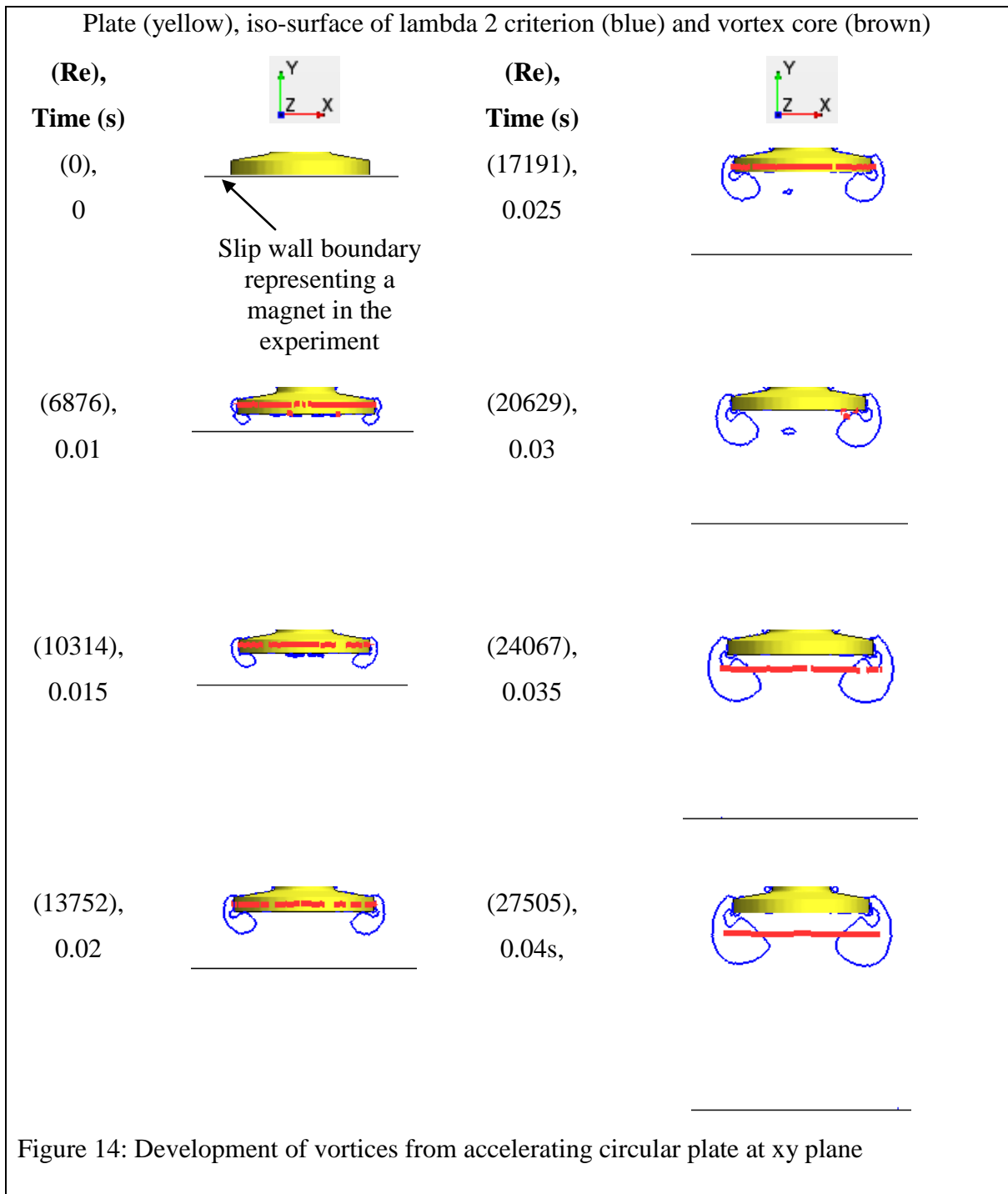
The points labelled A, B and C in Figure 13 are found in all Reynolds numbers (see Figure 10 to Figure 12). But at lower Reynolds numbers (Re), the flow features are very small to be identified and as Re increases they become more established. There is a relationship between Re and size of primary vortex. As Re increases, the shears layer A rolls into bigger primary vortex that have larger radius of curvature (see Figure 10 to Figure 12). The increase of Re also causes the vortex core B to simultaneously move in a negative y-direction (away from the plate) and radially outwards to accommodate the primary vortex that increases with Re .

In general, the experimental and CFD results are consistent with each other. The flow features A, B and C almost behave in the same way in both CFD and experiment. The laser shone from the right side of the plate hence the experimental vortex looks brighter on the right side of the axis. However, it can still be seen that primary vortex ring is axisymmetric. .

5.2.2. Development of the vortices around an accelerating circular plate

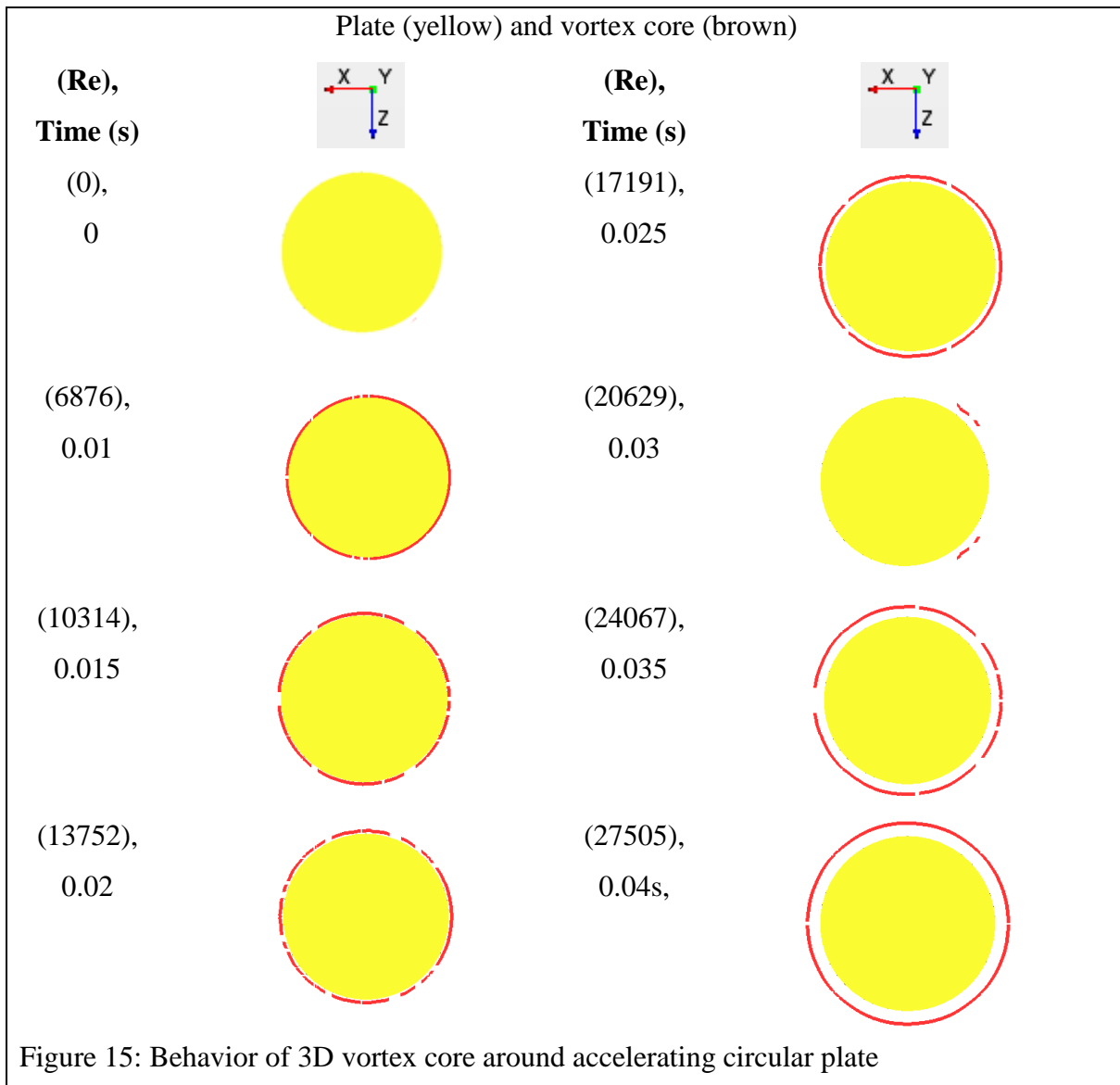
The velocity vector scene method discussed in Section 5.2.1 still identifies the vortex. However, the velocity vector scene is more on how the fluid particles in the domain generally behave during the plate motion. The CFD method of vortex identification shown in Figure 14

below is more on extracting the vortex in the domain. The iso-surfaces of lambda 2 criterion are used. This method would be used throughout the results discussion from now onwards.



In Figure 14 above, the primary vortex is shown in 2D (blue) while the vortex core is in 3D (brown). **Note** that in 2D and in Figure 14 above, the primary vortex appears to be two counter-rotating vortices on both sides of the y-axis. In actual fact and in 3D, the primary vortex is an axis-symmetric ring that results when 2D representation of vortex in Figure 14 is revolved around the y-axis through 360°. The 3D representation of primary vortex ring at various Reynolds numbers is shown in Figure 16, page 43.

As Re increases, the size of the primary vortex increases. The vortex core simultaneously moves in the direction of the wake and radially outwards to accommodate the growing vortex. The vortex core appears to be broken at some Reynolds numbers; this is due to the selection of parameters such as line width in CFD. In actual fact, the vortex core is supposed to be a continuous circle in the case of a circular plate. The results on Figure 14 above are consistent with the experimental and velocity vector scenes used for validation in Section 5.2.1



In order to accommodate the primary vortex ring that is growing with the Re in the wake direction, Figure 15 above shows the vortex core that increases in diameter. Figure 14 and Figure 16 show that the vortex core does not only increase in diameter but also moves in the wake direction as Re increases.

Plate (yellow), iso-surface of lambda 2 criterion in 3D (blue) and vortex core (brown)

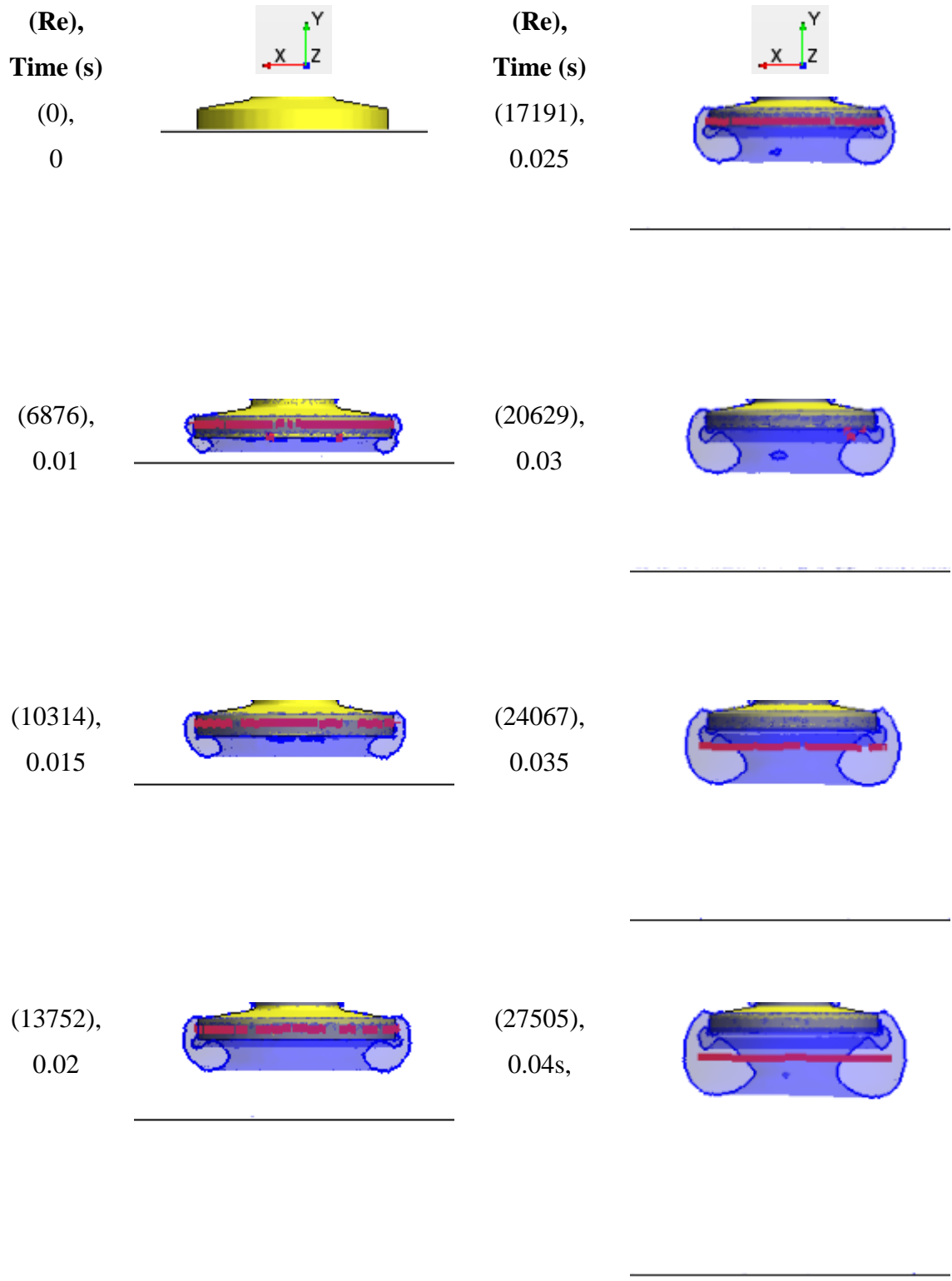


Figure 16: 3D development of vortices around accelerating circular plate

Figure 16 above shows the development of primary vortex around half of a circular plate in 3D. The relationship between 2D and 3D vortical representations can be seen; the 2D vortical structure from Figure 14 is visible on the 3D vortical structure. The vortex core is circular in shape (see Figure 15 above) and it simultaneously moves in a negative y-direction and radially outwards as Re increases. This vortex core behavior accommodates the increase of the size of the primary vortex that rolls around the vortex core as Re increases.

5.2.3. Summary of vortices shed by accelerating circular plate

A circular plate accelerating in air displaces air particles out of its way. These air particles are catapulted radially outwards as a shear layer and separate at the front edge (edge on the side with a shaft) of the plate. After separating, the shear layer rolls into an axis-symmetric primary vortex ring around a vortex core in the wake of the plate.

From Figure 10 to Figure 16, the relationship between the Reynolds number (Re) and the size of the primary vortex is displayed. As Re increases during the plate motion, the amount of fluid particles displaced from the front face of the plate also increases. As a result, the shear layer rolls into larger primary vortex around the vortex core. Briefly, the size of the primary vortex formed in the wake of the plate increases with the increasing Re . In order to accommodate the increasing size of the primary vortex, the vortex core increases in diameter with Re while at the same time translating in a wake direction (away from the plate).

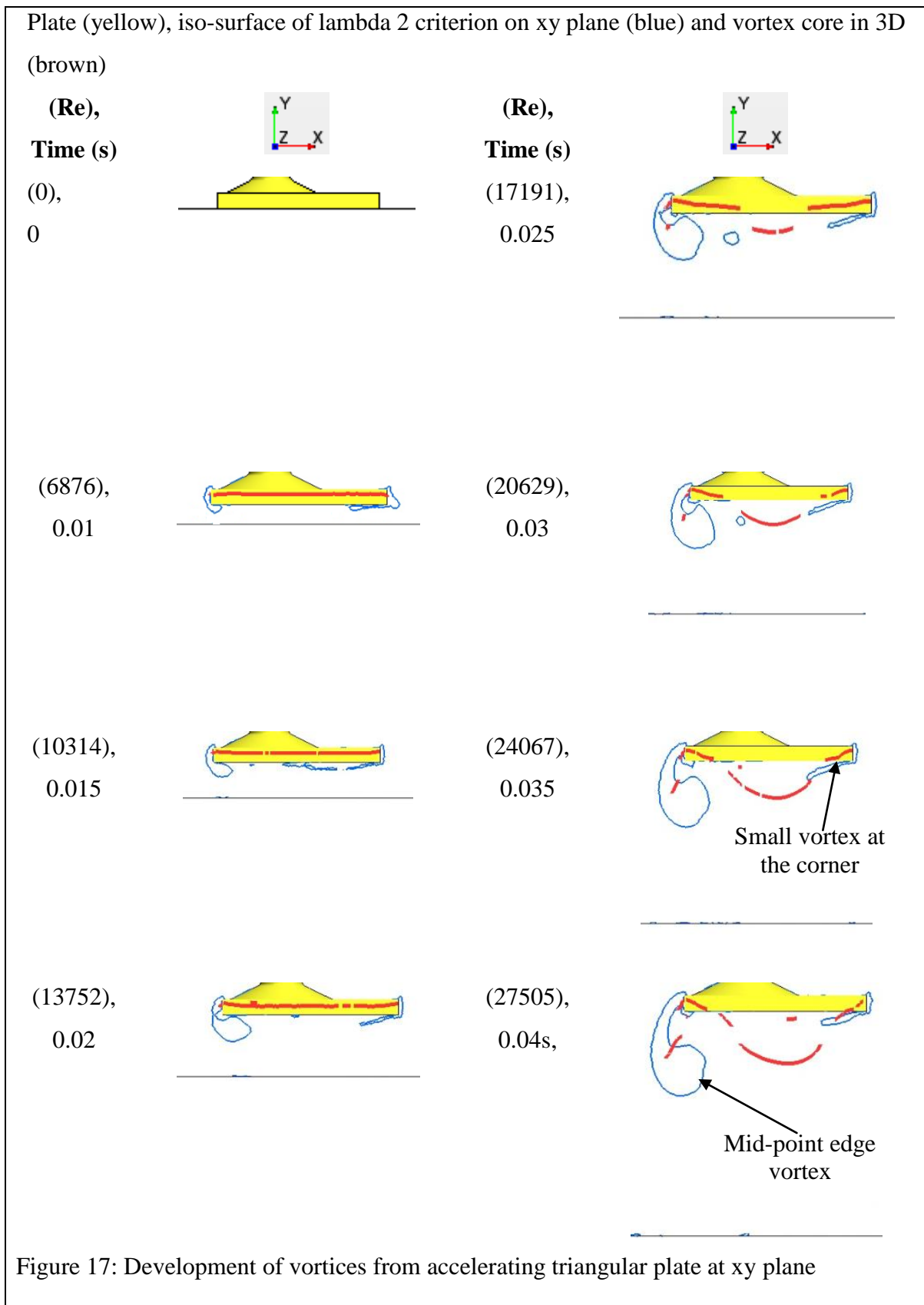
In 3D (Figure 16), the primary vortex is a tube or ring that wraps around a circular vortex core. This vortical structure is axis-symmetric; cutting any plane perpendicular to xz plane and passing through the plate centroid, the same vortical structure as represented on the xy plane in Figure 14 would be observed. The axis-symmetry of the primary vortex can be attributed to the circular or axis-symmetric shape of the front edge of separation.

5.3. Results of vortices shed by accelerating triangular plate

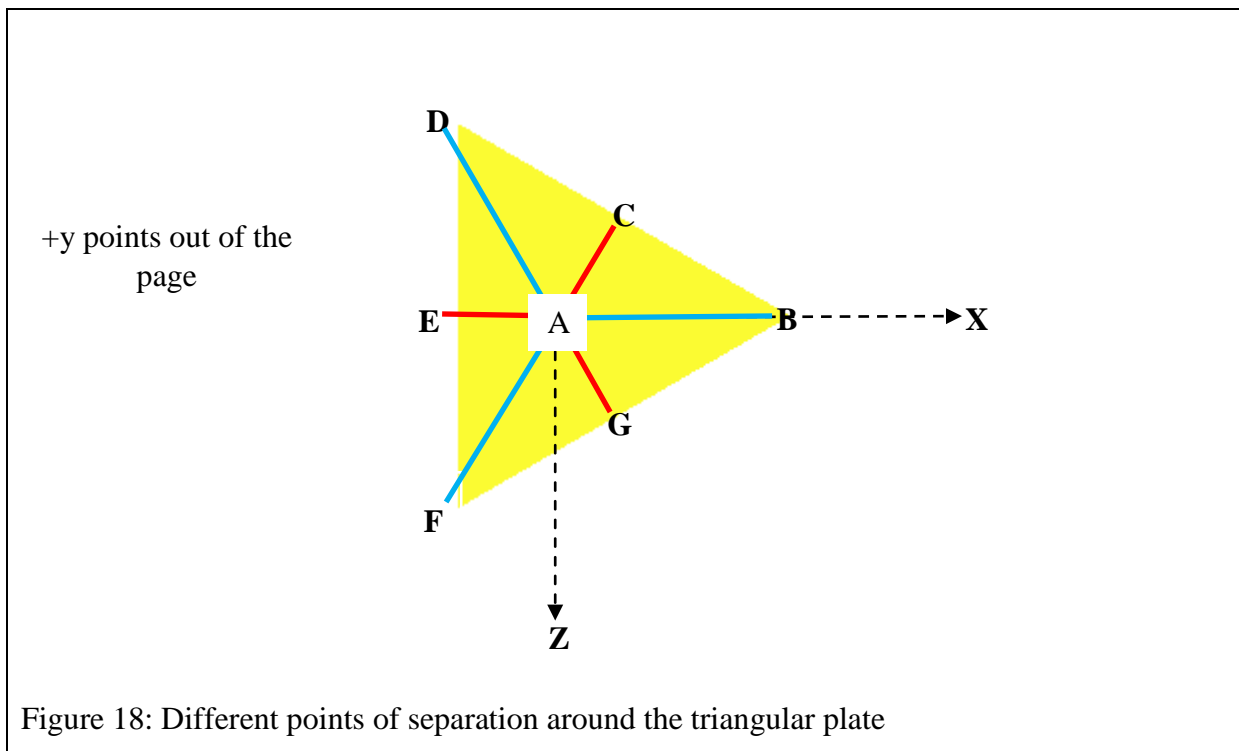
5.3.1. Validation of results for accelerating triangular plate

The simulation of the accelerating triangular plate was done with the same mesh, physics and boundary conditions that simulated a circular plate that was validated with an experiment. Therefore, the validation still holds for a triangular plate case.

5.3.2. Development of the vortices around an accelerating triangular plate



In Figure 17 above, the primary vortex is displayed by the iso-surfaces of lambda 2 criterion on xy plane (blue) while the vortex core is in 3D (brown). In 2D and at xy plane, the accelerating triangular plate leads to what appears to be two counter-rotating primary vortices of the different sizes. The vortex on the left side of the plate axis is at mid-point of the plate edge and it is bigger than the one on the right side of the axis which is at the corner of the plate. It is shown in Figure 20 page 50 that the primary vortex is, in actual fact, an asymmetric ring around the entire plate. Similar points of separation would display the same vortical structure in terms of size and shape at one instantaneous Reynolds number (Re). The importance of separation point on the vortical structure is explained using Figure 18 below.



There is an infinite number of separation points on the front edges (FEs) of the triangular plate. In Figure 18 above, the separation points at mid-points of the edges (C, E and G) and the centroid A are joined with a red line while corner separation points are joined with a blue line. The separation points joined by lines of the same colour are identical in terms of distance from the centroid and general appearance. The vortical structure shown on xy plane in Figure 17 is the result of fluid particles that separate at points B and E in Figure 18. It will be shown later that in 3D, the primary vortex is an asymmetric ring that is maximum around the plate mid-points of the edges (C, E and G). Going along the edges, from mid-points of the

edges to the corners (B, D and F), the vortex ring reduces in size. The shorter the distance from the plate centroid to the point of separation, the bigger the size of the vortical structure. The vortex ring would be maximum at mid-points (C, E and G) and continually reduces in size until it gets to the corners (B, D and F) where the size is smallest (see Figure 20 page 50 for 3D vortex representation).

As Re increases the size of the primary vortex increases and the vortex core simultaneously stretches in the direction of the wake. Going along the edges of the plate, the vortex core stretches more near the mid-points of the plate edges and keeps on approaching the plate until it gets to the corners where it is attached due to the smallest size of the vortical structure on the corners. This behavior of the vortex core accommodates the uneven or asymmetric growth of the primary vortex ring with increasing Re . The 3D primary vortex is shown in Figure 20 page 50 and vortex core in Figure 19 below.

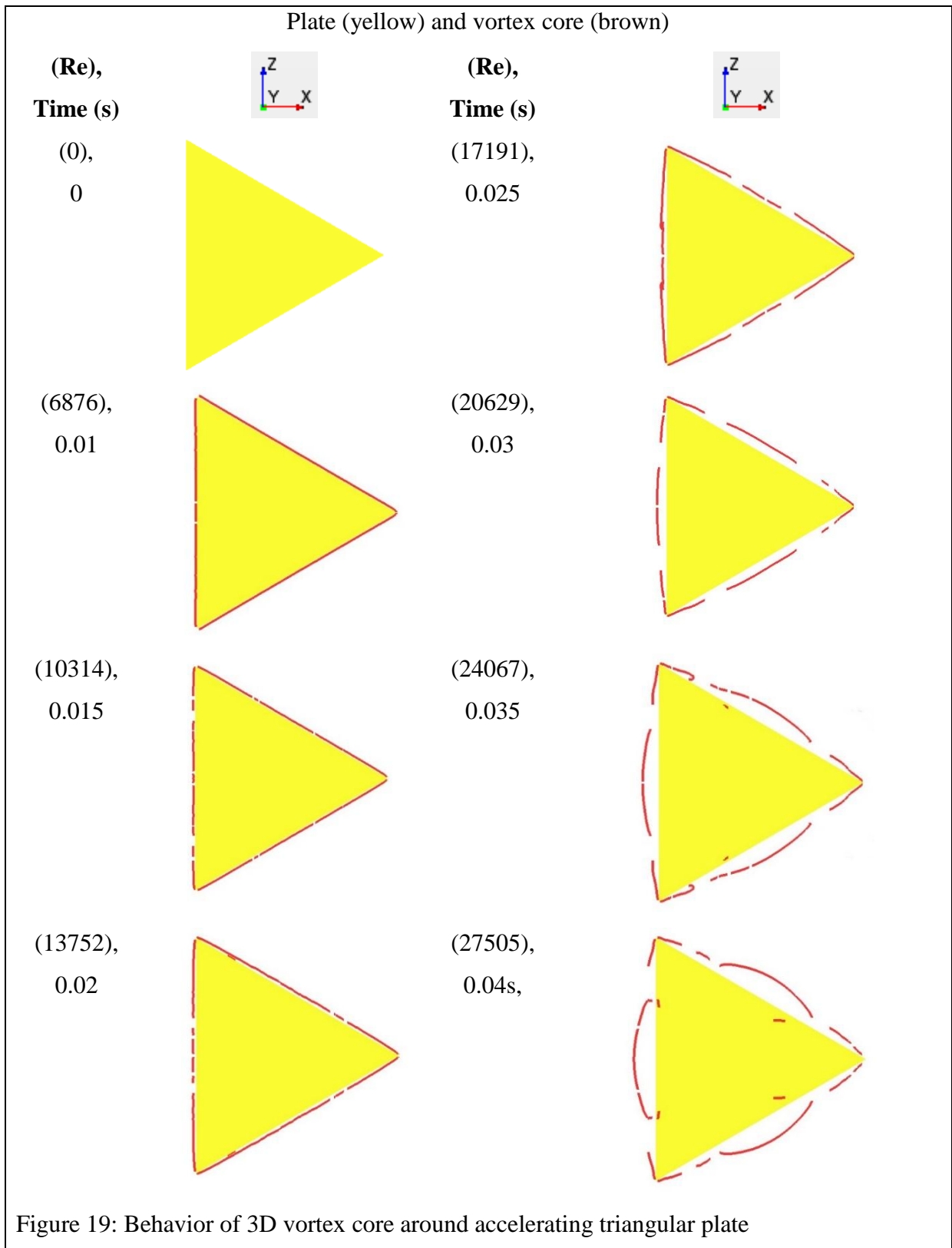


Figure 19 above shows that the vortex core is not only stretching in the wake direction (as it appears in Figure 17), but it also stretches in the radially-outward direction as Re increases. The way it stretches in the radial direction is not uniform; the stretch is more on the areas close to the mid-point of the edges. Going along the plate edges to the corners, the stretch is becoming less and less until at the corner where the vortex core is attached to the corners of the plate for all Reynolds numbers. The asymmetric behavior of the vortex core as Re increases is to accommodate the uneven or asymmetric growth of primary vortex that roll around it as shown in Figure 20 below.

It must be noted that the vortex core breaks along its length and this is due the CFD parameters used (such as line width of the core). In actual fact, the vortex core must be considered as a continuous.

Plate (yellow), iso-surface of lambda 2 criterion in 3D (blue) and vortex core (brown)

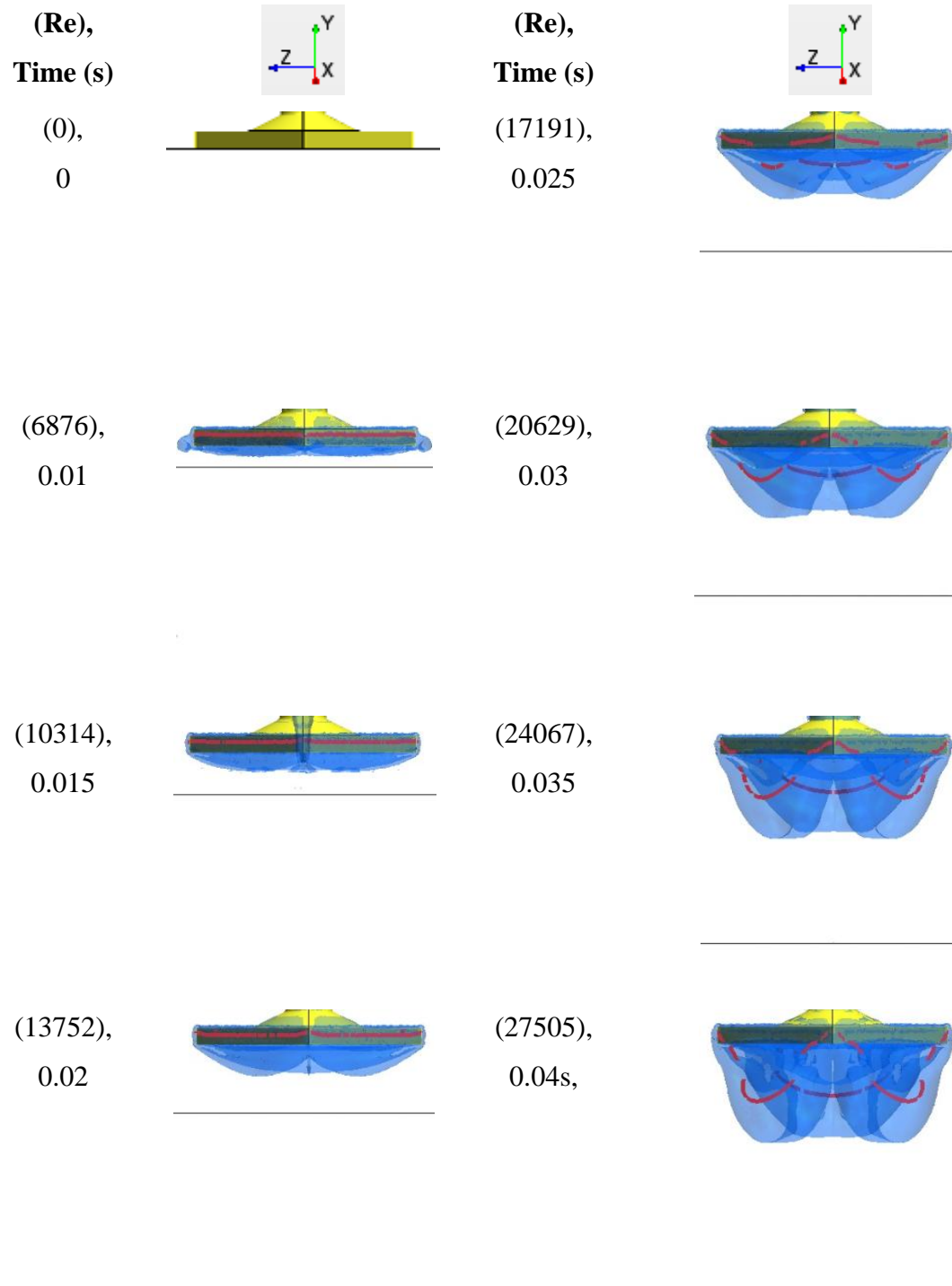
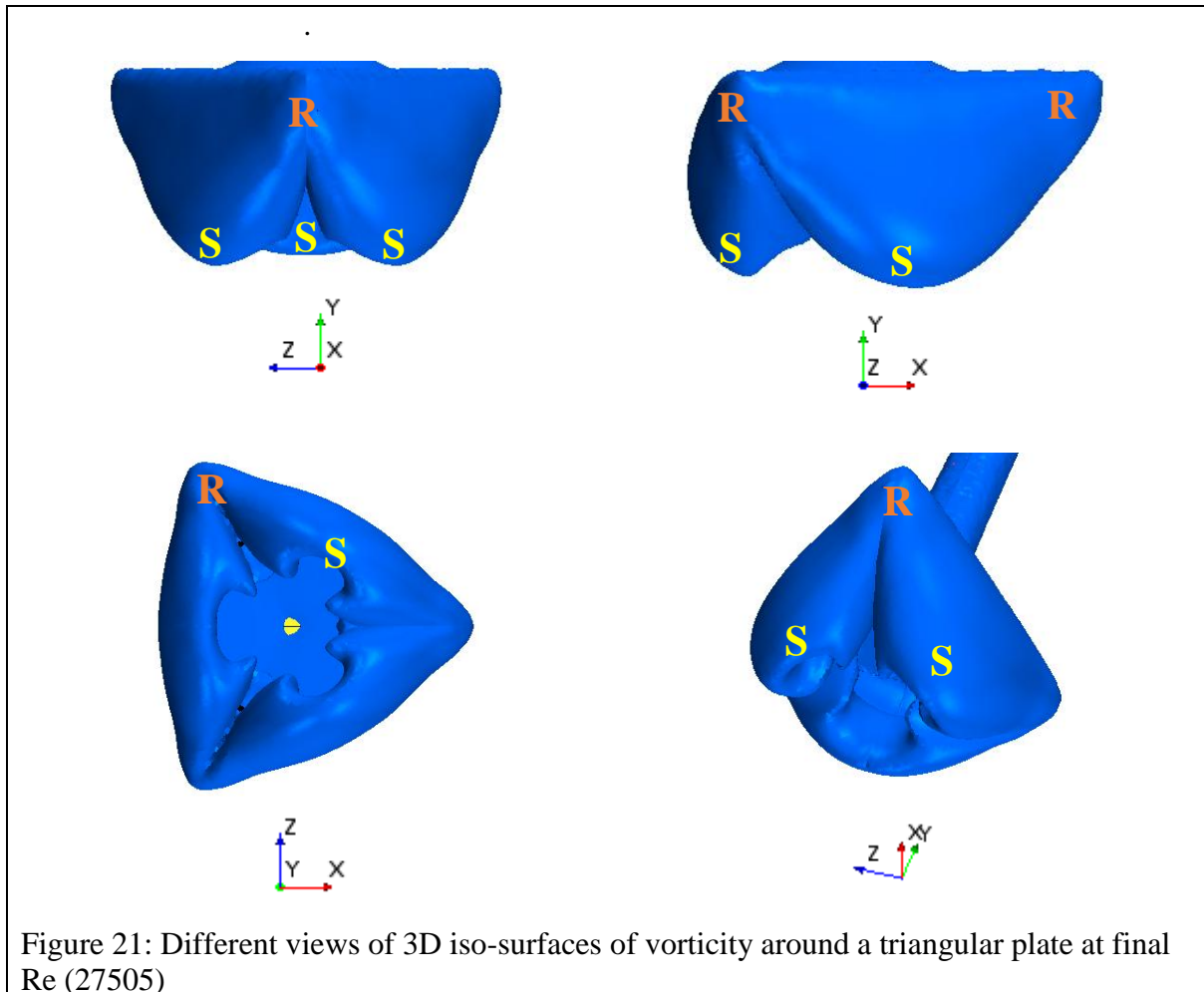


Figure 20: 3D development of vortices around accelerating triangular plate

5.3.3. Vortex behavior from the mid-points to the triangular plate corners

The behavior of a primary vortex ring, going along the edges from the three mid-points to the three corners, is shown on Figure 21 below at final Re where the ring is maximum:



From Figure 21 above:

- The iso-surfaces of vorticity (blue) are shown in 3D at different views; the opacity is maximum and the vortex core is not visible inside the ring.
- The primary vortex is an asymmetric ring that starts from the plate edges and rolls in the wake side of the plate
- S is the biggest part of the primary vortex ring close to the mid-points of the triangular plate edges.
- R is the smallest part of the primary vortex ring at the corners of the plate.
- The size of the primary vortex ring continuously reduces from the three mid-points of the plate edges to the three corners.

- The parts of the primary vortex ring from two edges connects at the corner joining those two edges

5.3.4. Summary of vortices shed by an accelerating triangular plate

A triangular plate accelerating in air displaces air particles out of its way. These air particles are catapulted radially outwards as a shear layer and separate at the front edges of the triangular plate. After separating, the shear layer rolls in the wake of the plate forming asymmetric primary vortex ring around a vortex core. At unique instantaneous Re , the vortex ring is at its maximum from the three mid-points of the three edges of the plate. Going along the edges from the mid-points to the three corners of the plate, the primary vortex ring continuously reduces in size. The vortex ring from two edges of the plate interacts or connects at the corner joining those edges.

To summarise the vortex shedding from square plate, let:

- Re_1 be a unique instantaneous Reynolds number and Re_2 be the next instantaneous Reynolds number ($Re_1 < Re_2$).
- P_1 be the amount of air particles being displaced from the plate at Re_1 and P_2 be the amount of air particles being displaced at Re_2 ($P_1 < P_2$)
- PVR_1 be a general size of primary vortex ring at Re_1 and PVR_2 be the size of primary vortex ring at Re_2

When Re increases from Re_1 to Re_2 , the amount of air particles displaced by the plate at a time increases from P_1 to P_2 . P_2 rolls into a primary vortex ring PVR_2 that is greater in size than PVR_1 . Briefly, the size of primary vortex formed at the wake of the plate increases with the increasing Re . This is because the plate velocity increases with Re leading to an increase in amount of air particles that can be displaced at a time.

Uneven growth of primary vortex can be attributed to asymmetry of the points of separation around a triangular plate. The points of separation, which are on the triangular edges, are physically different. Even at a one Reynolds number, some air particles would be separating at the corners while others at the edges. It can be argued that even at a plate edge, there are infinite number of separation points that are physically different. For instance, the point of separation at the mid-point of the plate edge is physically different from the point closer to the corner in terms of distance from the plate centroid.

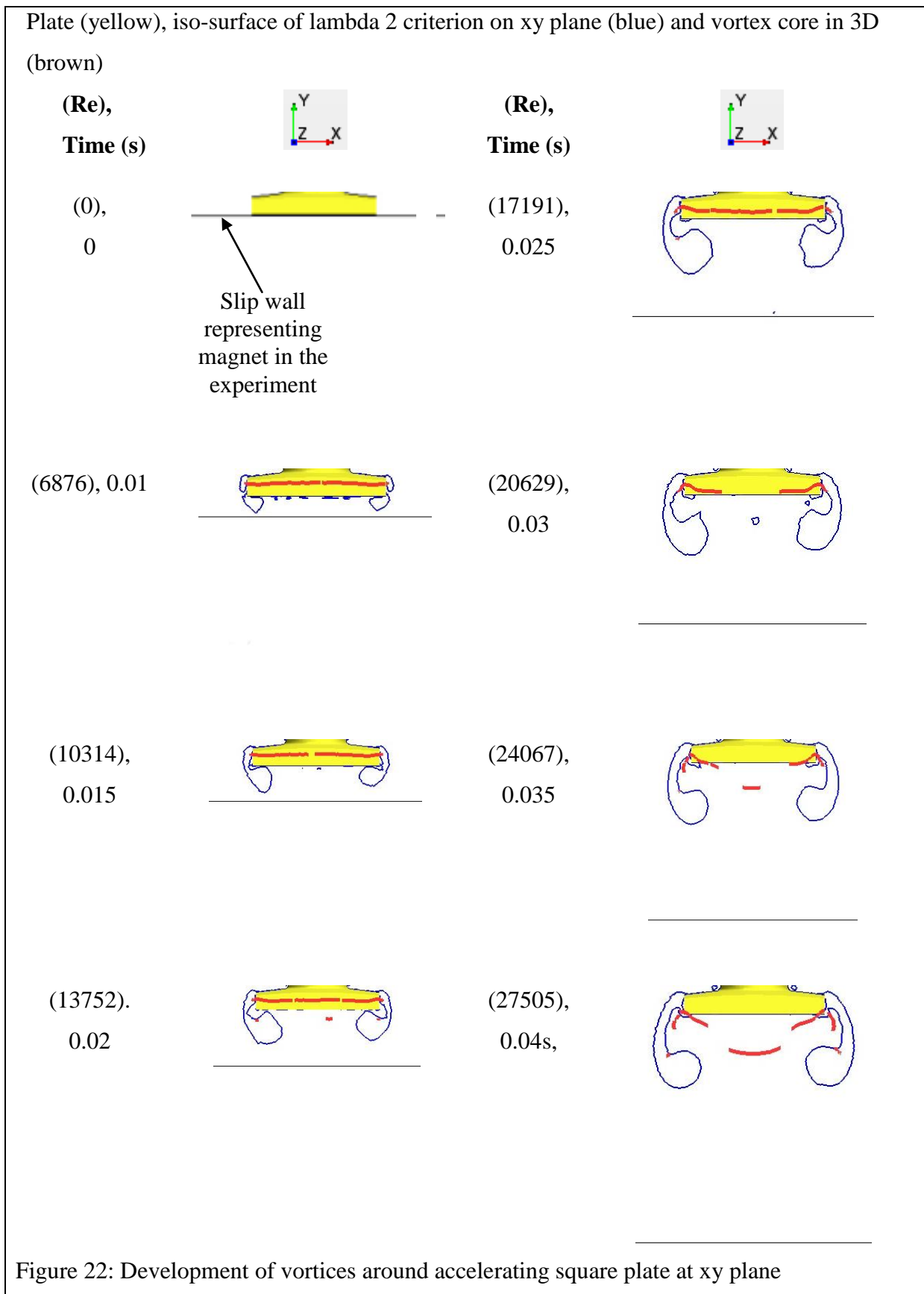
The asymmetry of the region of separation leads to shear layer separating from the triangular plate in a different manner or momentum. The observation is that the shear layer rolls in to vortical structure of highest curvature at the mid-points of the edges of the asymmetric plates. Going from the mid-points of the plate edges to the corners, the size of primary vortical structure continuously reduces in size until it gets to the corners.

5.4.Results of vortices shed by accelerating square plate

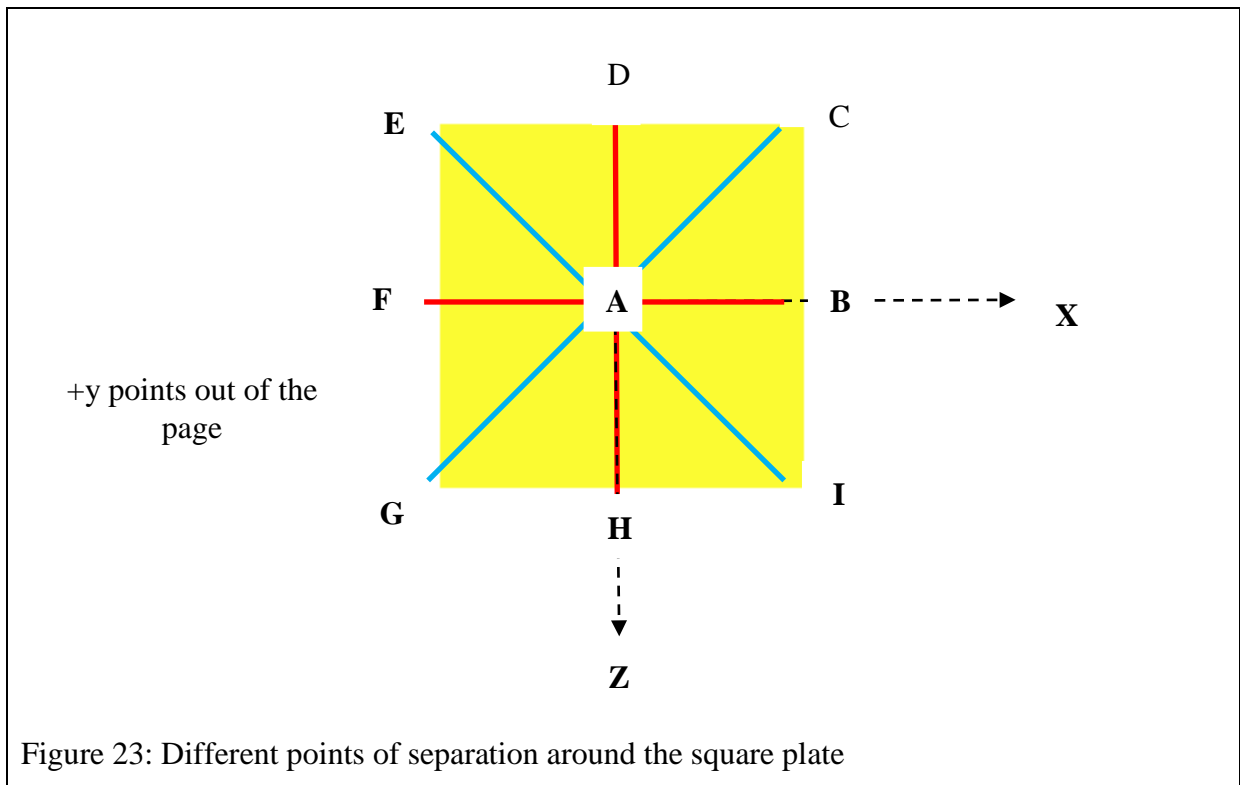
5.4.1. Validation of results for accelerating square plate

The simulation of the accelerating square plate was done with the same mesh, physics and boundary conditions that simulated a circular plate that was validated with an experiment. Therefore, the validation still holds for a square plate case.

5.4.2. Development of the vortices around accelerating square plate



In Figure 22 above, the vortex is displayed by iso-surfaces of lambda 2 criterion on xy plane (blue) while the vortex core is in 3D (brown). In 2D and at xy plane, the accelerating square plate leads to what appears to be two counter-rotating primary vortices of the same size; the vortex on the left side of the plate axis is the mirror image of the one on the right. It is shown on Figure 25 page 59 that the primary vortex is, in actual fact, an asymmetric ring around the entire plate. It is just that two similar points of separation would display the same vortical structure in terms of size and shape at one instantaneous Reynolds number (Re). The importance of separation point on the vortical structure is explained using Figure 23 below.



There are an infinite number of separation points on the front edges (FEs) of the square plate. In Figure 23 above, the separation points at mid-points of the edges (B, D, F and H) and the centroid A are joined with a red line while corner separation points are joined with a blue line. The separation points joined by similar line are identical in terms of distance from the centroid and general appearance. The vortical structure shown on xy plane in Figure 22 is the result of air particles that separate at points B and F in Figure 23. It will be shown later that in 3D, the primary vortex is an asymmetric ring that is maximum around the plate mid-points of the edges (B, D, F and H). Going along the edges, from mid-points of the edges to the corners (C, E, G and I), the vortex ring reduces in size. The shorter the distance from the plate centroid, the bigger the size of the vortical structure. The vortex ring would be maximum at

mid-points (B, D, F and H) and continually reduces in size until it gets to the corners (C, E, G and I) where the size is smallest (see Figure 25).

As Re increases, the size of the primary vortex increases and the vortex core simultaneously stretches in the direction of the wake. Going along the edges of the plate, vortex core stretches more near the mid-points of the plate edges and keeps on approaching the plate until it gets to the corners where it is attached due to the smallest size of the vortical structure on the corners. This behavior of the vortex core accommodates the uneven or asymmetric growth of the primary vortex ring with increasing Re . The 3D primary vortex is shown in Figure 25 on page 59 and vortex core in Figure 24 below.

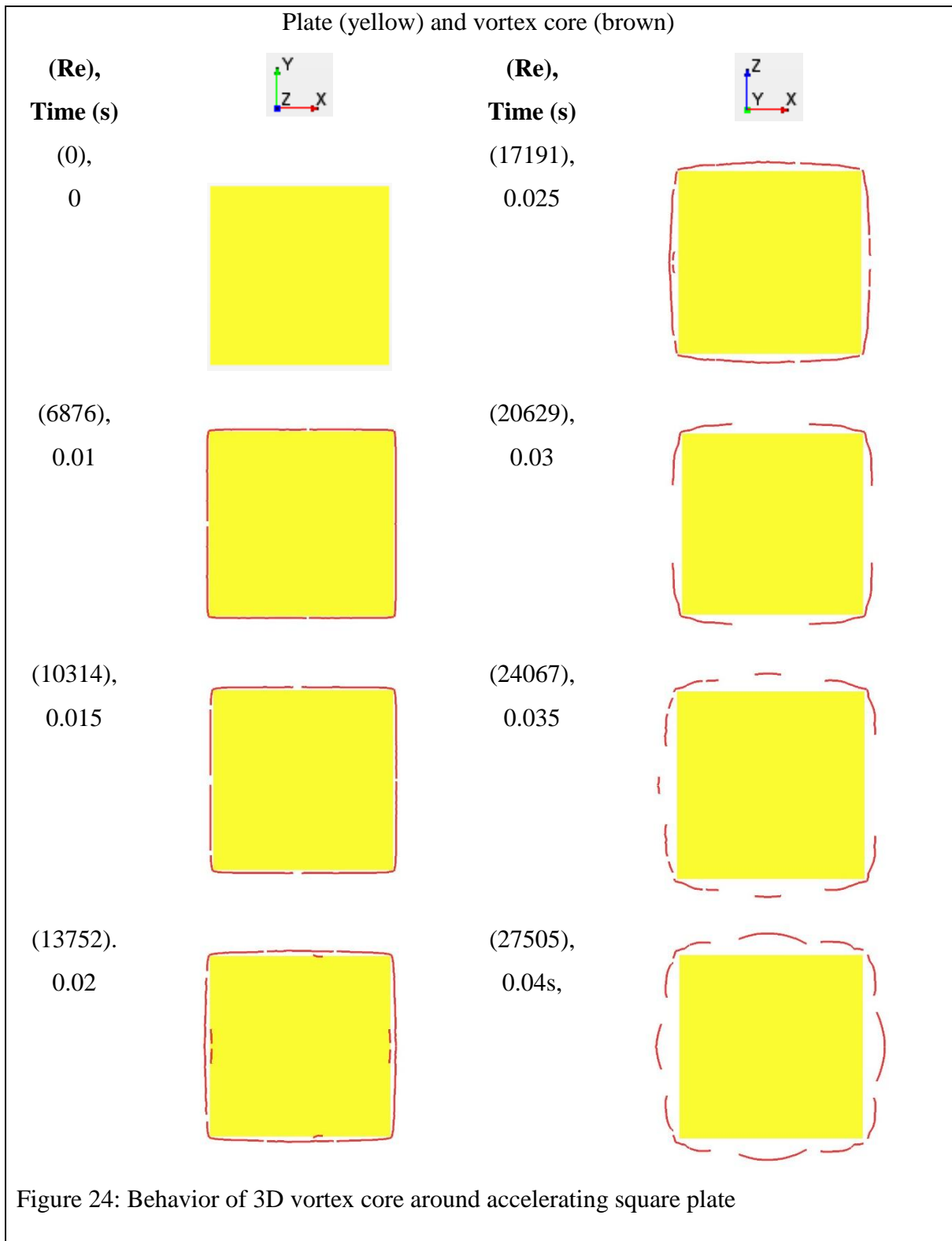


Figure 24 above shows that the vortex core is not only stretching in the wake direction (as shown in Figure 22), but it also stretches in the radially-outward direction as Re increases. The way it stretches in the radial direction is not uniform; the stretch is more on the areas close to the mid-points of the edges. Going along the plate edges from the mid-points of the edges to the corners, the stretch becomes less and less until at the corners where the vortex core is attached to the corners of the plate. The behavior of the vortex core as Re increases accommodates the uneven growth of primary vortex that rolls around it as shown in Figure 25 below.

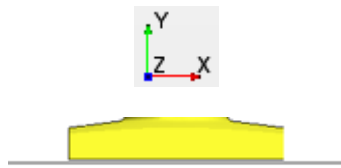
It must be noted that the vortex core breaks along its length and this is due the CFD parameters used (such as line width of the core). In actual fact, the vortex core must be considered as a continuous.

Plate (yellow), iso-surface of lambda 2 criterion in 3D (blue) and vortex core in 3D

(brown)

(Re),
Time (s)

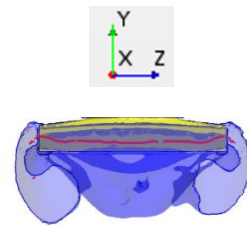
(0),
0



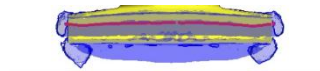
Slip wall
representing
magnet in the
experiment

(Re),
Time (s)

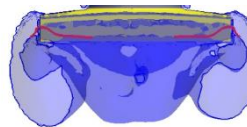
(17191),
0.025



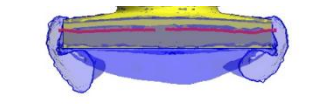
(6876),
0.01



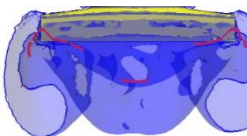
(20629),
0.03



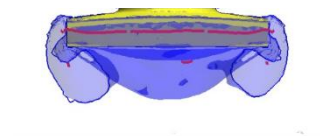
(10314),
0.015



(24067),
0.035



(13752),
0.02



(27505),
0.04s,

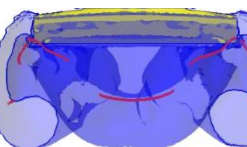
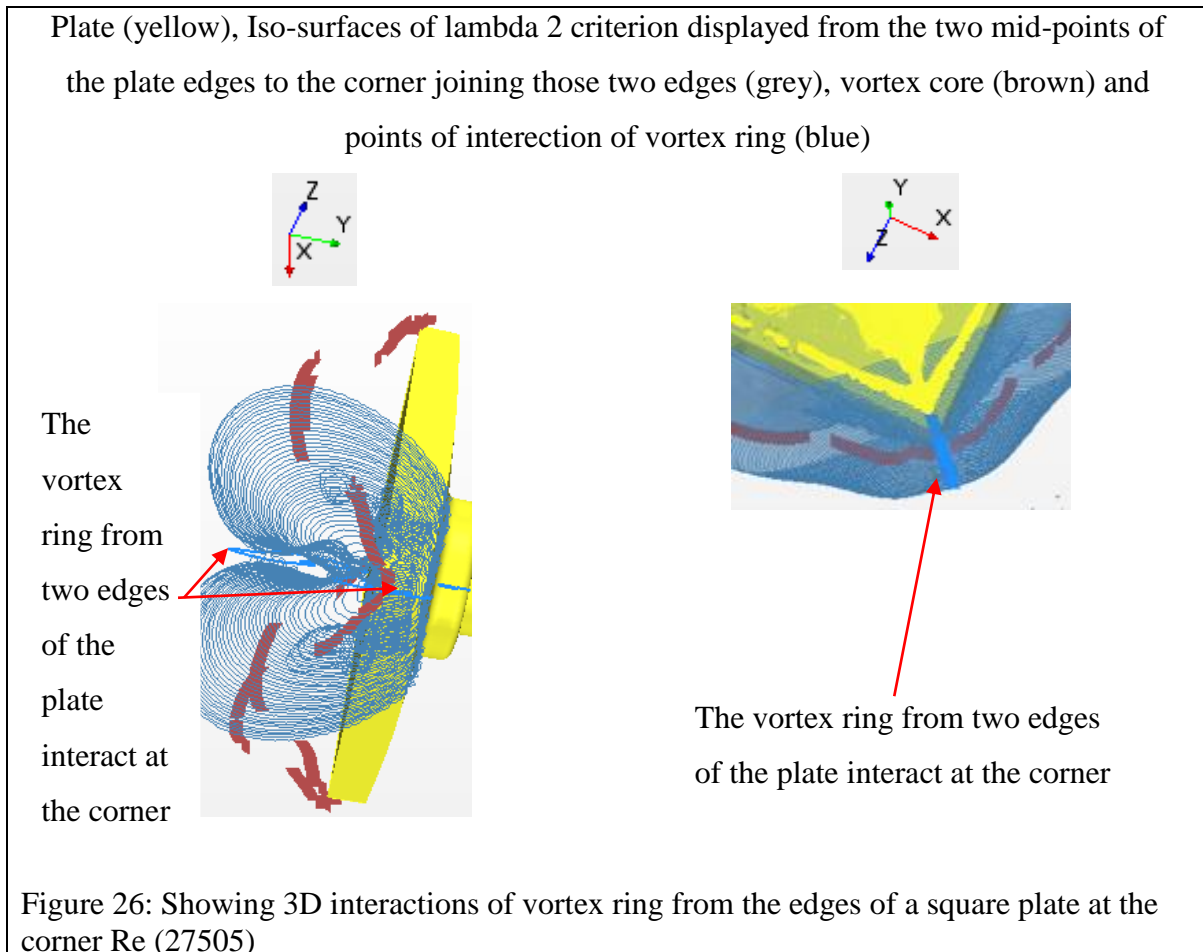


Figure 25: 3D development of vortices around accelerating square plate

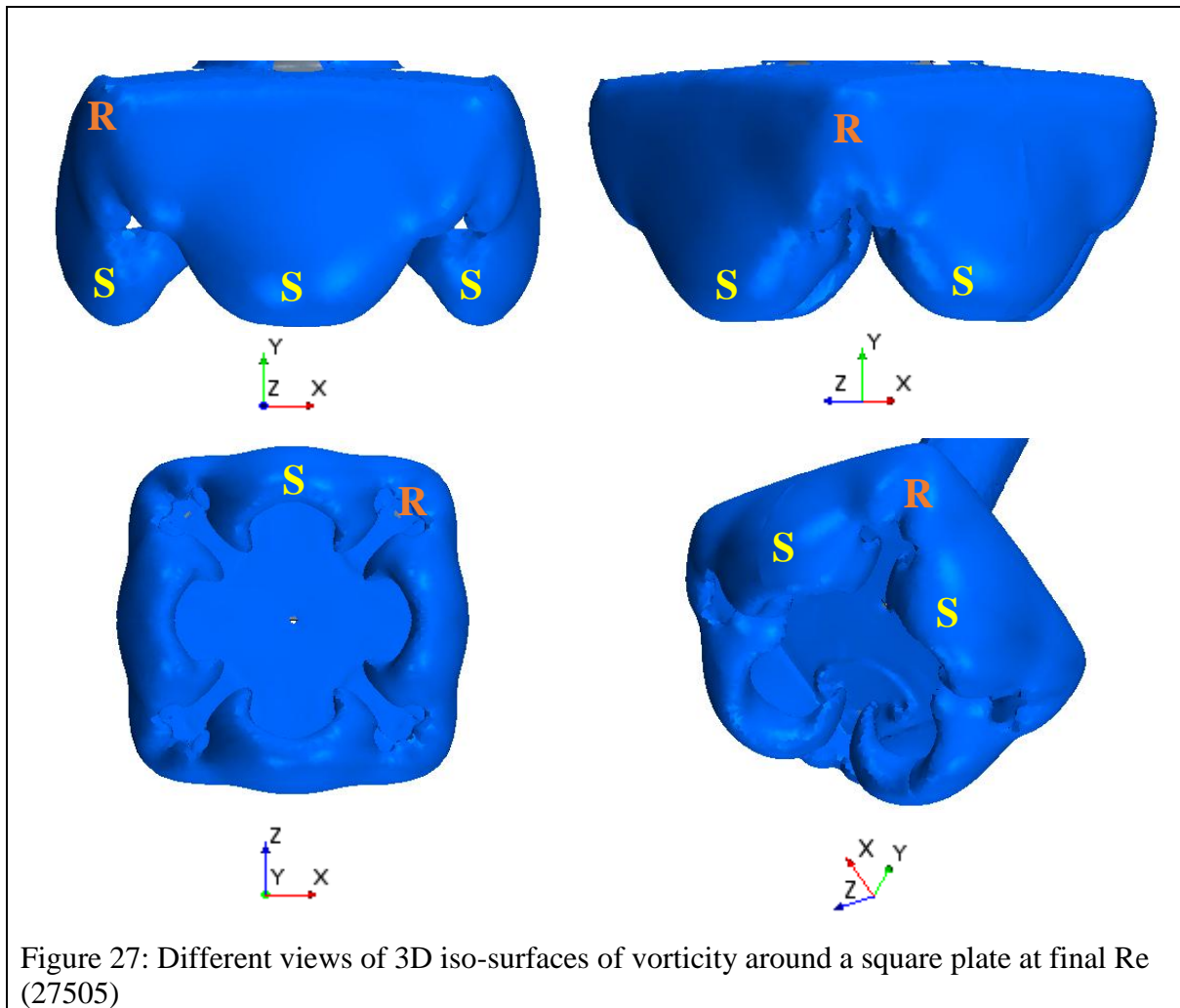
5.4.3. Behavior of vortex from the mid-points to the corners of the square plate

The behavior of a primary vortex ring, going along the edges from the four mid-points to the four corners, is shown in Figure 26 and Figure 27 below at final Re where the ring is maximum:



From Figure 26 above:

- The iso-lines of lambda 2 criterion (grey) are shown from the two mid-points of the square plate edges to the corner that connects those edges. Vortex core can be seen through the iso-lines that are displayed on many section planes.
- The size of the primary vortex ring continuously reduces from the mid-points of the plate edges to the corner joining those edges.



From Figure 27 above:

- The iso-surfaces of vorticity (blue) are shown in 3D at different views; the opacity is maximum and vortex core is not visible inside the vortex ring.
- The primary vortex is an asymmetric ring that starts from the plate edges and rolls in the wake side of the plate
- S is the biggest part of the primary vortex ring close to the mid-points of the square plate edges.
- R is the smallest part of the primary vortex ring at the corners of the plate.
- The size of the primary vortex ring continuously reduces from the four mid-points of the plate edges to the four corners.
- The parts of the primary vortex ring from two edges connects at the corner joining those two edges

5.4.4. Summary of vortices shed by accelerating square plate

A square plate accelerating in air displaces air particles out of its way. These air particles are catapulted radially outwards as a shear layer and separate at the front edges of the square plate. After separating, the shear layer rolls in the wake of the plate forming asymmetric primary vortex ring around a vortex core. At unique instantaneous Re , the vortex ring is maximum from the four mid-points of the four edges of the plate. Going along the edges from the mid-points to the four corners of the plate, the primary vortex ring continuously reduces in size. The vortex ring from two edges of the plate interacts or connects at the corner joining those edges.

To summarise the vortex shedding from square plate, let:

- Re_1 be a unique instantaneous Reynolds number and Re_2 be the next instantaneous Reynolds number ($Re_1 < Re_2$).
- P_1 be amount of air particles being displaced from the plate at Re_1 and P_2 be the amount of air particles being displaced at Re_2 ($P_1 < P_2$)
- PVR_1 be a general size of primary vortex ring at Re_1 and PVR_2 be the size of primary vortex ring at Re_2

When Re increases from Re_1 to Re_2 , the amount of air particles displaced by the plate at a time increases from P_1 to P_2 . P_2 rolls into a primary vortex ring PVR_2 that is greater in size than PVR_1 . Briefly, the size of primary vortex formed at the wake of the plate increases with the increasing Re . This is because the plate velocity increases with Re leading to an increase in the amount of air particles that can be displaced at a time.

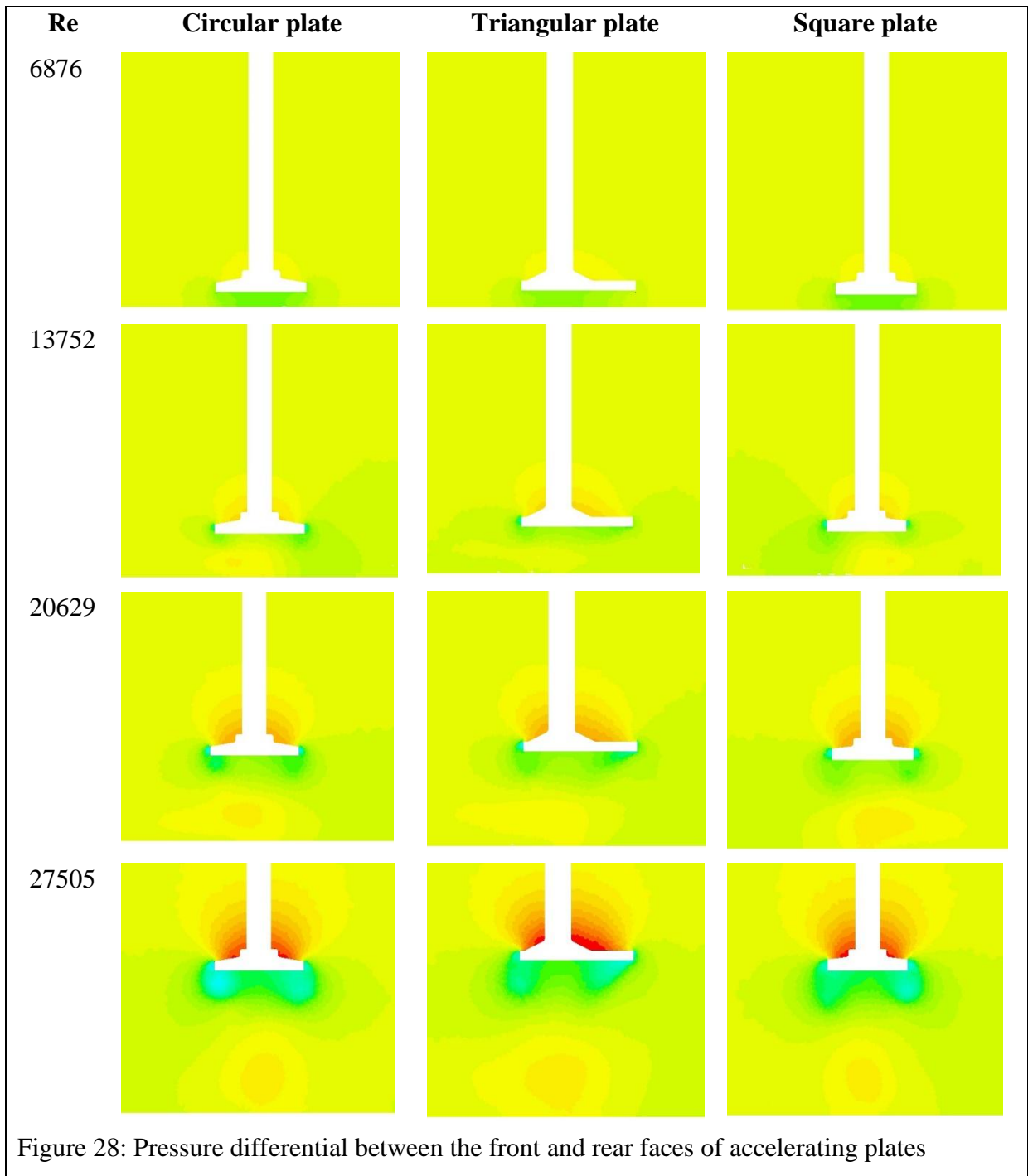
Uneven growth of primary vortex can be attributed to asymmetry of the points of separation around a square plate. The points of separation, which are on the square edges, are physically different. Even at a one Reynolds number, some air particles would be separating at the corners while others at the edges. It can be argued that even at one plate edge, there are infinite number of separation points that are physically different. For instance, the point of separation at the mid-point of the plate edge is physically different from the point closer to the corner in terms of distance from the plate centroid.

The asymmetry of the region of separation leads to shear layer separating from the square plate in a different manner or momentum. The observation is that the shear layer rolls in to vortical structure of highest curvature at the mid-points of the edges of the asymmetric plates. Going from the mid-points of the plate edges to the corners, the size of the primary vortical structure continuously reduce in size until they get to the corners.

5.5.Drag force from accelerating plates

Lee et. al., [20] experimentally investigated free stream acceleration effects on drag force in bluff bodies using a wind tunnel. They found that the additional momentum due to acceleration increased the drag on bluff bodies with sharp edges. In this project the same additional momentum due to acceleration has been related to the momentum of separating shear layers hence the increase of resulting primary vortex during the acceleration and increase in Reynolds number.

The size of vortex was found to increase with Reynolds number (Re) in the wake of the accelerating plate. Figure 28 below shows that the pressure differential between the front and rear faces of the accelerating plates increases with Reynolds number (Re). As Re increases, the pressure on the front face of the plate increases and pressure drops more in the wake of the plate. The maximum pressure drop is where the vorticity is highest. This increase in pressure differential leads to increasing drag force experienced by plates during the motion as can be seen on Figure 29. These results are consistent with findings of Lee et. al., [20] where additional momentum due to acceleration was found to cause the increase in drag forces on bluff bodies with edges.



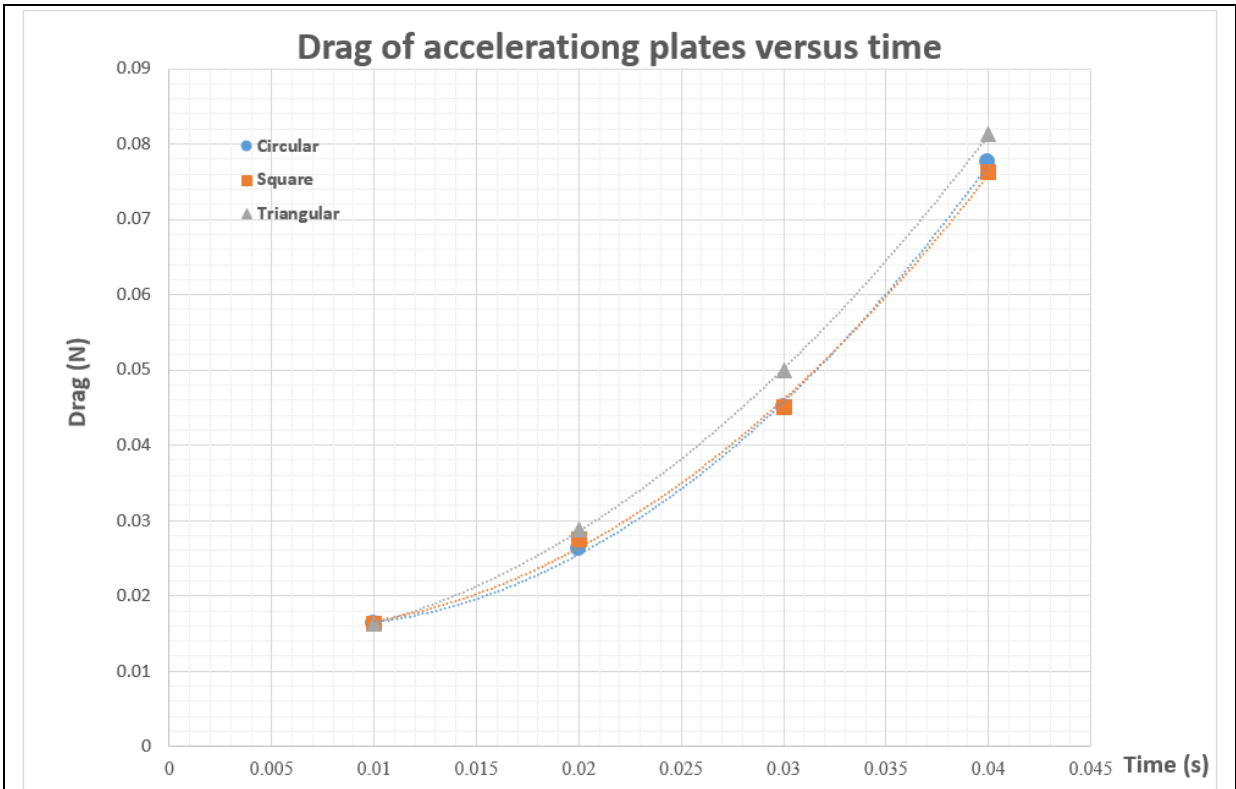


Figure 29: Drag force of accelerating plate versus time

5.6. Experimental Challenges

This section discusses the challenges and limitations encountered during the experiment. The pressure regulator on the experimental rig could be set to a maximum of 10 bar. Referring to the findings of Rosi and Rival [19], that increasing acceleration lead to “Kelvin Helmholtz (KH) instability being clearer and more organized”, it would be advisable to use the acceleration that was as high as possible to visualise more visible and organised vortices shed by plates. That is, the typical pressure to be set in this experiment would be that maximum 10 bar because the highest pressure set on the system would give the highest acceleration of the plates that might produce clearer vortices

However, the pressure was set to 2 bar (20 % of the maximum pressure that could be set on the pressure regulator). Referring to section 3.4 page 16 step 13, it can be remembered that electro-magnet control was working as a starter for the plate to accelerate in the experiment. When the magnet control was turned off, the electromagnet lost its magnetism hence the pressurized plate that was tightly attracted to the magnet started accelerating due to the pressure in the rig system. In the current experimental set-up, it was found that once the

pressure was set to 3 bar upwards, the force pushing the plate and piston upwards was greater than the attractive force from the electro magnet. Thus, the plate would leave the magnet before the magnet control was turned off. In order to have a total control of when to start the plate motion by using a magnet control, the pressure (in this case 2 bar) that would produce a force that was just less than the attractive force from the magnet had to be chosen. Therefore higher pressures could not be set on the pressure regulator.

The FSR triggering sensor had to be in contact between the plate and electromagnet in order to function. The FSR with its thickness of about 1 mm, did not allow for 100% contact between the plate and magnet thereby creating a small gap. The gap was reducing the effectiveness of the attractive force of the magnet on the plate. This point ties to the recommendation for repeating the experiment “the triggering sensor that allows for 100% contact of plate and magnet is recommended”.

The continuous 1W laser in the Wits University Flow Research Unit did not produce enough light for flow profiles to be captured. Then the solution was to rent a 2W laser from LaserX Company for R4000 per day. The current experiment was very demanding in terms of time. Many trials had to be made when trying to get the right amount of smoke to make visible vortex. The price for renting a laser was too high considering the budget for completing the project. As a result, the testing was limited to a few days due to the limit of the budget. The budget could only allow the author to get results for accelerating circular plates only. More experimental results could not be achieved in the case of triangular and square plates. Therefore the validation of the CFD results was based on a circular plate only. It was assumed that applying the same CFD method that has been validated with axis-symmetric or circular plate to square and triangular plates would still give reliable results to conclude about those asymmetric plates.

It was expected that the uniform smoke in the smoke box would produce more visible vortex. This was not the case; letting the smoke to be uniform was not producing clearer flow profiles of accelerating plate as can be seen on Figure 30 below. The plate had to be accelerated before the smoke could be uniform or when there was a smoke turbulence going on. The latter option produced some visible vortices (right image of Figure 30 below). However, it was difficult to visualise the vortex shedding brought by accelerating plate inside the unwanted disturbances caused by the smoke turbulence.

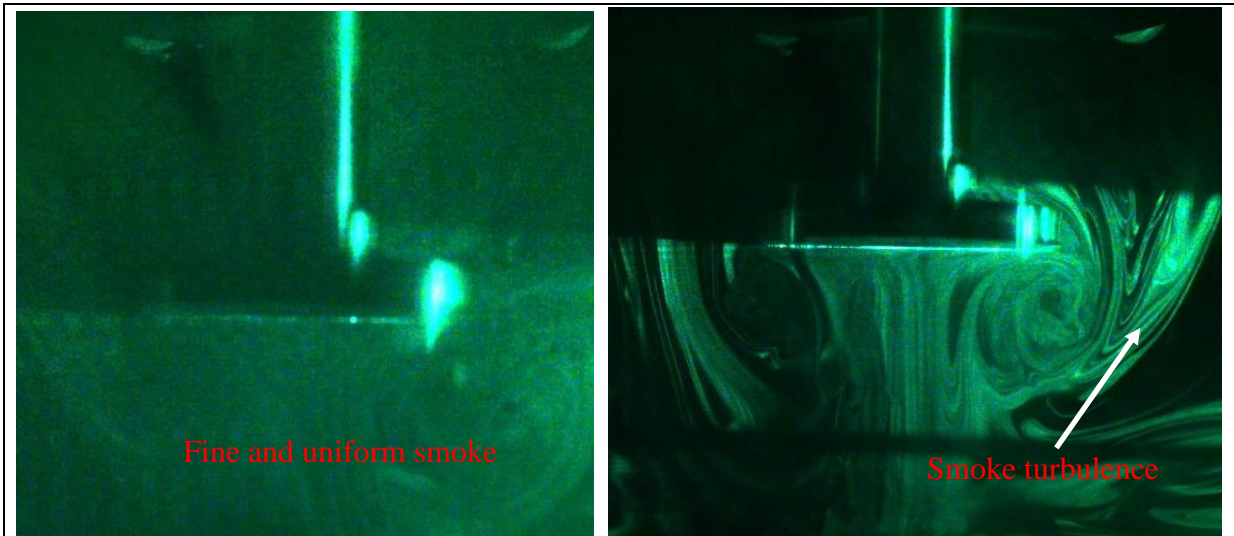


Figure 30: Fine and uniform smoke not producing clear and visible vortices (left) and smoke with turbulence producing visible vortex (right)

5.7. Computational Challenges

The overset mesh with zero gap interface has been successfully used to simulate the plates accelerating with constant acceleration from rest. The overset gap interface worked very well as the geometry was made in such a way that the end of the shaft extended out of the domain (see Figure 5 in page 20). This could not be achieved by normal overset mesh that does not allow the boundaries to overlap each other. The capability of overset zero gap interface that allowed overset mesh to extend outside the domain successfully managed to simulate the current problem.

However, the overset mesh creates a temporary wall where boundaries overlap or where there is a gap less than four cells between boundaries. In the current simulation the overset mesh and shaft wall boundary was in contact with the background from the beginning to the end of simulation to allow for that shaft to extend outside the domain. The temporary wall between shaft wall boundary, overset and background regions negatively affected the mesh quality but to an acceptable level.

Chapter 6: Conclusion and recommendation

6.1. Conclusion

The overset mesh simulation in Star CCM+ was successfully validated using the laser vapor sheet experiment and it managed to give the results about the vortices shed by rapidly accelerating plates. Therefore this CFD method can be used to simulate complex fluid flow problems that accelerate rapidly in air and shed the vortices, like accelerating missiles and planes. The following conclusions were drawn about plates accelerating uniformly from rest with a uniform acceleration of 13 g and from Reynolds number 0 to 27505.

6.1.1. Accelerating plates in general

- Reynolds number increases constantly during the uniform acceleration of the plate
- As a plate accelerates in air, it displaces air particles out of its way and catapult them radially outwards from its front face. The air particles separate as a shear layer from the front edges of the plate. The shear layer rolls in the wake of the plate forming a primary vortex ring around a vortex core.
- The size of the primary vortex increases with Reynolds number. As Reynolds number increases, more air particles are displaced from the front face of the plate at a time. More particles lead to a shear layer that separates with high momentum resulting into larger primary vortex.
- The vortex core increases, or stretches, with increasing Reynolds number in such a way that accommodates the primary vortex ring that wrap around it as it grows with increasing Reynolds number.
- The shape of the vortex core is dependent on the shape of the accelerating plate and it changes with Reynolds number to accommodate the unique growth of vortex from a certain plate.
- The drag force experienced by an accelerating plate increases with Reynolds number. The pressure differential between the front and rear faces of the accelerating plate increases with Reynolds number resulting in an overall increase in drag force.
- The maximum pressure drop at the wake of the plate is around the areas of maximum vorticity.

6.1.2. Accelerating axis-symmetric plates

- A circular plate leads to axis-symmetric ring of primary vortex around a circular vortex core.
- The vortex core starts as a circle of diameter equal to that of a plate and as Reynolds number increases it continually increases in diameter and translates in the wake direction to accommodate the axis-symmetric growth of primary vortex.
- The axis-symmetric primary vortex is attributed to the axis symmetric separation region. The air particles are distributed evenly as they are catapulted from the front face of the plate and they separate in a same way from a circular or axis symmetric separation region or edge. The result is axis-symmetric primary vortex around the plate

6.1.3. Accelerating non-axis-symmetric plates

- Accelerating asymmetric (square or triangular) plates leads to asymmetric primary vortex ring. The size of primary vortex ring close to the mid-points of the plate edges is maximum and going along the plate edges, the vortex ring reduces in size from the mid points of the edges to the corners of the plate.
- The asymmetric shape of primary vortex around triangular and square plates are attributed to asymmetry of the region or edges of separation from those plates. Region of separation is a square or triangular edge on the front face of the plate. Infinite number of separation points on these edges are physically different; some air particles would be separating at the corners and some on the plate edges. Different separation points lead to uneven vortical structure due to the different ways at which air particles would separate from the plate.
- In order to accommodate uneven growth of primary vortex along the edges of the asymmetric plates, vortex core stretches more on areas close to the mid-points of the plate edges. Going from the mid-points of the edges to the corners, the vortex core keeps on going closer and closer to the plate until it reaches the corners where it is attached due the smallest primary vortices at the corners.
- The vortex ring from the edges of the plates interact at the corner of the plate joining those edges.

6.2.Recommendations

- The validation of the investigation was done by doing experiment on the circular or symmetric plate only. The validation can be strengthened by performing further experiments even on the asymmetric plates (square and triangular plates).
- The triggering sensor used in this project had to be in contact between the plate and magnet. The gap created by this 1 mm sensor reduced the effectiveness of the magnet in terms of attracting the plate towards it. Therefore, a sensor that is not reducing the effectiveness of the magnet is recommended so that higher pressures can be set on the pressure regulator to allow for higher accelerations hence being able to reach higher Reynolds numbers. This can allow for the investigation of the vortex dynamics of the accelerating plate at higher Reynolds numbers where the primary vortex gets advected and breaks down into secondary vortices. The secondary instability on the wake of accelerating plates has never been investigated in 3D according to the literature accessed by the author.
- To reduce the turbulence of the smoke, more visualisation methods must be tried in order to obtain results when the smoke is very fine and uniform.

References

- [1] I. M. Gledhill, K. Forsberg, P. Eliasson, J. Baloyi and J. Nordstrom, "Investigation of acceleration effects on missile aerodynamics using Computational Fluid Dynamics," *Aerospace Science and Technology*, vol. 13, no. 4 - 5, pp. 197 - 203, 2009.
- [2] P. A. Blackmore, "The effects of aircraft trailing vortices on house roofs," *Journal of Wind Engineering and Industrial Aerodynamics*, vol. 52, pp. 155 - 170, 1994.
- [3] W. Leqin, M. Xudan, L. Zhifeng, W. Peng and W. Dazhuan, "Simulations of the transient flow generated from a started flat plate," *Chinese Journal of Mechanical Engineering*, vol. 25, no. 6, pp. 1190 - 1197, 2012.
- [4] T. Colonius and D. R. Willams, "Control of vortex shedding on two- and three-dimensional airfoils," Mechanical and Aerospace Engineering Department of California Institute of Technology and Illinois Institute of Technology, Pasadena CA and Chicago IL, 2011.
- [5] K. Schneider, M. Paget-Goy, A. Verga and M. Farge, "Numerical simulation of flows past flat plate using volume penalization," *Comp. Appl. Math.*, 2014.
- [6] S. Taneda, "Visual study of unsteady separated flows around bodies," *Prog. Aerospace Sci*, vol. 17, pp. 287 - 348, 1977.
- [7] Z. J. Wang, "Vortex shedding and the frequency selection in flapping flight," *J. Fluid Mech*, vol. 410, pp. 323 - 341, 200.
- [8] H. Roohani and B. W. Skews, "Investigation of the effects of acceleration on aerofoil dynamics," in *In the 5th South African Conference on Computational and Applied Mechanics (SACAM 06)*, Cape Town, January 16 - 18, 2006.
- [9] A. Sayma, Computational Fluid Dynamics, 2009. [E-book] Available: <http://bookboon.com/en/computational-fluid-dynamics-ebook> [Accessed 29 March 2016].
- [10] H. K. Versteeg and W. Malalasekera, Computational Fluid Dynamics The Finite Volume Method, Essex England: Longmand Scientific and Technical, 1995.
- [11] K. M. Singh, "Computational Fluid Dynamics NPTEL Mechanical Engineering CFD Course," IIT Roorkee, [Online]. Available: <http://nptel.ac.in/courses/112107080/>. [Accessed 29 Mar. 2016].
- [12] T J Birch, I. E. Wrisdale and S. A. Prince, "CFD Predictions of Missile Flow Fields," *AIAA 2000 - 4211*, 2000.
- [13] H. Roohni, "Aerodynamic effects of accelerating objects in air," University of the Witwatersrand, Johannesburg, 2010.
- [14] Q. You, S. Fang and L. Zhu, "Visualizing Vortex Shedding of an Elastic Plate Interacting with a 3D Viscous Flow," in *IEEE Ninth International Conference on Computer and Information Technology*, Indianapolis, USA.
- [15] M. Jiang, R. Machiraju and D. Thompson, "Detection and visualisation of vortices," The Ohio State University Department of Computer and Information Technology and Mississippi State University Department of Aerospace Engineering.
- [16] V. Holmen, 'Methods for vortex identification', MSc Eng. Mathematics, Numerical Methods and Fluid Mechanics, Lundi University, 2012.

- [17] J. L. Colehour and B. W. Farquhar, "Inlet vortex," *Journal of Aircraft*, vol. 8, no. 1, pp. 39 - 43, 25 08 1971.
- [18] P. Koumoutsakos and D. Shiels, "Simulations of the viscous flow normal to an impulsively started and uniformly accelerated flat plate," *J. Fluid Mech*, vol. 328, pp. 177 - 227, 1996.
- [19] G. A. Rosi and D. E. Rival, "Entrainment and topology of accelerating shear layers," *J. Fluid Mech*, vol. 811, pp. 37 - 50, 2017.
- [20] Y. Lee, J. Rho, K. H. Kim and D. H. lee, "Fundamentals Studies on Free Stream Acceleration Effect on Drag Force in Bluff Bodies," *Journal of Mechanical Science and Technology*, vol. 25, no. 3, pp. 695 - 701, 2011.
- [21] S. Mahjoob, M. Mani and M. Taeibi-Rahni, "Aerodynamic Performance Analysis of Bodies with Different Cross-Sections," in *20th AIAA Applied Aerodynamics Conference*, St Louis, Missouri, 24 - 26 June 2002.
- [22] M. Falchi, G. Provenzano, D. Pietrogiacomi, G.P. Romano, "Experimental and numerical investigation of flow control on bluff bodies by passive ventilation," *Experiments in Fluids*, vol. 41, pp. 21 - 33, 2006.
- [23] Y. A. Cengel and J. M. Cimbala, "Fluid Mechanics Fundamentals and Applications," New York, McGraw-Hill, 2006, pp. 561 - 598.
- [24] "Star CCM+ Version 10.04 User Guide," CD Adapco, Melville NY, 2015.
- [25] I. M. A. Gledhill, H. Roohani, K. Forsberg, P. Eliasson, B. W. Skews and J. Nordstrom, "Theoretical treatment of fluid flow for accelerating bodies," *Theor. Comp. Fluid Dyn.*, vol. 30, pp. 449 - 467, 2016.
- [26] D. Mann, "STAR-CCM+ v9.06 Preview: Overset Mesh with Zero Gap Interface," CD-Adapco, 27 Oct. 2014. [Online]. Available: <http://www.cd-adapco.com/blog/david-mann/star-ccm-v906-preview-overset-mesh-zero-gap-interface>. [Accessed 30 Mar. 2016].
- [27] D. C. Wilcox, *Turbulence Modelling for CFD 2nd Edition*, California: DCW Industris, Inc, 1998.
- [28] "Learn Engineering," [Online]. Available: <http://www.learnengineering.org/2013/08/fluid-thermal-fundamentals.html>. [Accessed 21 Jun. 2015].
- [29] "LearnCAX," Centre for Computational Technologies, [Online]. Available: <https://www.learncax.com/class/www/student.php>. [Accessed 01 August 2015].
- [30] J. Hu, et al, "Validation of Turbulence Models in Star- CCM+ by N.A.C.A. 23012 Airfoil Characteristics," in *ASEE Northeast Section Conference*, Bridgeport, CT, 2009.
- [31] V. Mali, "Basics of Y Plus, Boundary Layer and Wall Function in Turbulent Flows," LearnCAX, [Online]. Available: <https://www.learncax.com/knowledge-base/blog/by-category/cfd/basics-of-y-plus-boundary-layer-and-wall-function-in-turbulent-flows>. [Accessed 19 Oct. 2015].
- [32] M. Ariff, S. M. Salim and S. C. Cheah, "Wall Y+ Approach for Dealing with Turbulent Flow over a Surface Mounted Cube: Part 2 - High Reynolds Number," Department of Mechanical, Materials and Manufacturing Engineering , University of Nottingham (Malaysia Campus), Semenyih in Malaysia, 2009.
- [33] V. J. Rossow, "Lift-generated vortex wakes of subsonic transport aircraft," *Progress in Aerospace Science*, vol. 35, pp. 507 - 660, 1999.
- [34] C. R. Nelson and B. M. Babie, *Flow Visualization by Direct Injection Technique*, Dept.

Aero., University of Notre Dame, Notr Dame, IN, USA: John Wiley & Sons, Ltd, 2010.

- [35] N. M. a. B. W. Skews, "Laser Vapour Screens Visualisation of Three - Dimensional Compressible Flow Fields," University of the Witwatersrand, Johannesburg, 2005.
- [36] S. I. Yaniger, "Force Sensing Resistors: A Review of the Technology," IEEE Xplore, [Online]. Available: <http://ieeexplore.ieee.org/stamp/stamp.jsp?tp=&arnumber=718294>. [Accessed 18 Apr. 2016].
- [37] "Arduino," [Online]. Available: <http://www.arduino.org/products/boards/arduino-uno>. [Accessed 17 Jan. 2017].
- [38] P. L. Davis, A. T. Rinehimer and M. Uddin, "A Comparison of RANS-Based Turbulence Modelling for Flow over a Wall-Mounted Square Cylinder," N C Motorsports and Automotive Research Center, Department of Mechanical Engineering and Engineering Science, The University of North Carolina, Charlotte in USA.
- [39] D. Christiaan, Interviewee, *Airfoil Rotating Using Overset Meshing*. [Interview]. 26 June 2015.
- [40] "Our best-in-class solvers and comprehensive physics models cover all flow regimes," CD-Adapco, [Online]. Available: <http://www.cd-adapco.com/products/star-ccm%C2%AE/solvers>. [Accessed 24 Oct. 2015].
- [41] R. F. Hanby, D. J. Silvester and J. W. Chew, "A Comparison of coupled and segregated iterative solution techniques for incompressible swirling flow," *International Journal for Numerical Methods in Fluids*, vol. 22, pp. 353 - 373, 1996.
- [42] J. Bairstow, "Flow Dynamics around Rapidly Accelerated Flat Plates," University of the Witwatersrand, Johannesburg, 2014.

Appendix

Appendix 1: Specifications for the apparatus used

Table 4: Pressure regulator specification [42]

Manufacturer	Shako
Model number	UFR/L-04
Operating pressure range	0.5 – 10 kgf/ cm ²
Max. flow rate	2600 l/min
Ambient temperature	-10 – 60 °C

Table 5: Vacuum pump specification

Model number	1550 – V1368
Voltage	220V
Current	5A
Frequency	50Hz
Power	0.75kW

Table 6: Electro-magnet specification [42]

Manufacturer	Lifton magnets Ptc Ltd
Product name	Electromicro
Model number	EMF3515
Voltage input	220VAC
Voltage output	110VDC
Magnetic force	9 – 12 kg/cm ²

Table 7: Electro – magnet control chunk specification [42]

Manufacturer	Holidings electronics Co... Ltd
Model number	WL-115C
Voltage input	220VAC
Voltage output	110VDC

Table 8: 2W – Laser specification

2W (2000mW) Green Diode laser @ 520nm with beam divergence of <math><1.2 \times 0.4 \text{ mrad}</math>. Flat plane was been scanned at 60000 pps from the software the image had 60 points in it

Table 9: FSR specification [39]

Force	1 – 20N
Pressure	10.3kPa – 1MPa
Repeatability Error Max	$\pm 2\%$
Sensing area	14.5 cm ²
Life span	10 million actuations
Operating temperatures	-30 – 70 °C
Response time max	3 μ s
Note: Program for triggering the camera is in the appendix	

High Speed Camera

Table 10: Photron FASTCAM SA5 high speed camera specification [42]

Model number	775K – C1
Image sensor	CMOS image sensor
Maximum resolution	1024 x 1024 pixels
Frame rate	50 – 1000000 fps
Recording memory capacity	8/16/32GB
Trigger signal	transistor – transistor logic (TTL)

Appendix 2: Triggering circuit and program code for triggering a high speed camera

The idea of Arduino which is an open source (from the reference [37]) has been used to build this circuit.

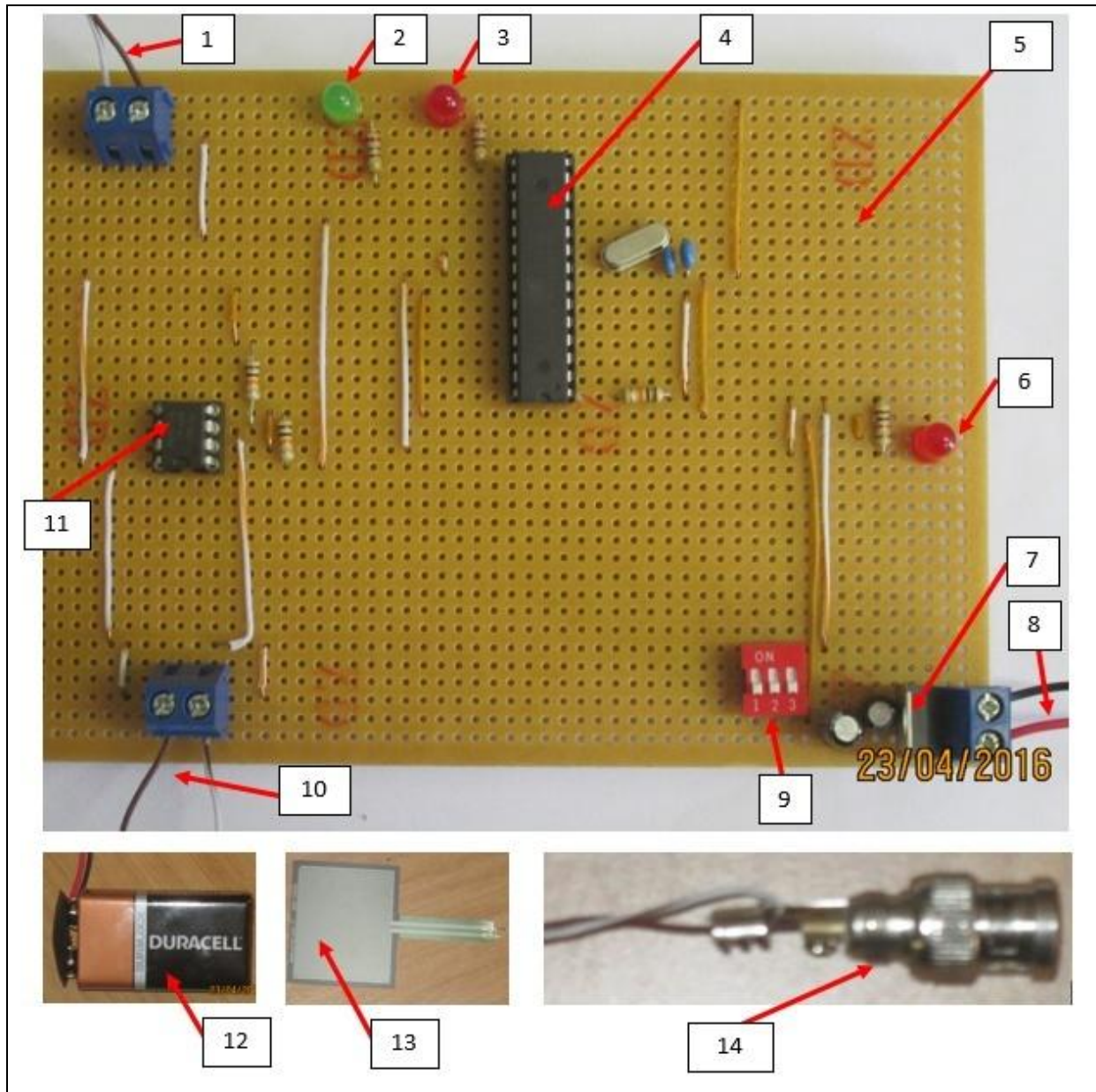


Figure 31: Photo of triggering circuit used

1 = two cables to BNC: for sending 5V from the circuit to a camera to trigger it

2 = green LED: indicates when FSR is experiencing no force

3 = red LED: indicates when FSR is experiencing force

4 = Micro-controller: in-puts the output of the amplifier and depending on whether the FSR is experiencing force or not, red or green LED will light; that is 5V is sent to the camera only when FSR experiences no force

5 = Vero board: board for building electric circuits

6 = 5V indicator

7 = Regulator: takes 9V@250mA and converts it to 5V@250mA required by micro-controller

8 = power input: two cables to 9V battery

9 = ON/OFF switch

10 = two cables to FSR

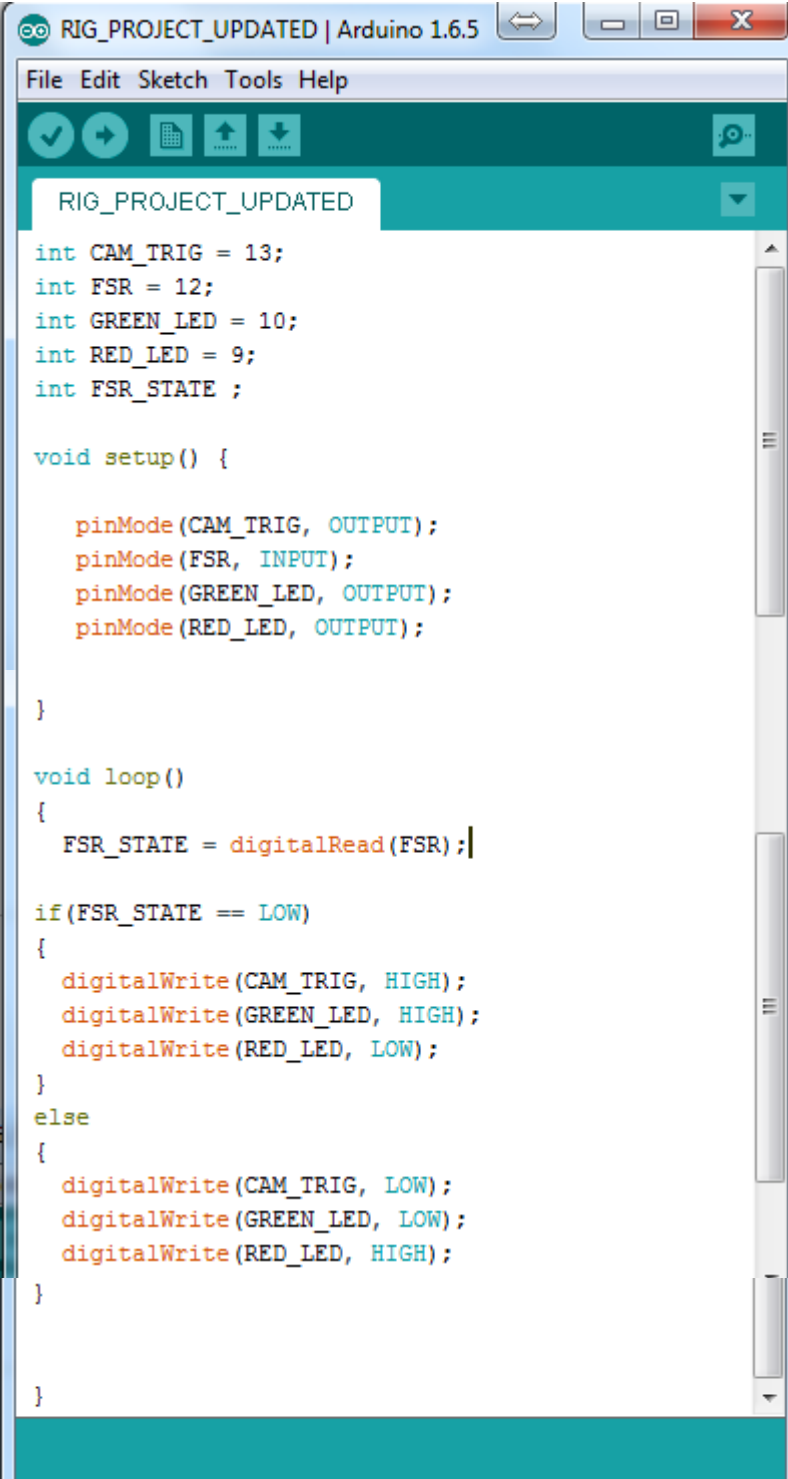
11 = Operational amplifier LM358 (OP – AMP): changes analogue signal to digital signal that is in a form of LOW and HIGH signal output

12 = 9V battery for power input

13 = Force Resistive Sensor (FSR): lowers in resistance when experiencing force and increases resistance when experiencing no force

9V at 250mA is supplied from battery 12 to the circuit through two cables 8. The regulator 7 converts 9V at 250mA into 5V at 250mA which is required by micro – controller 4. OP-AMP 11 is configured as an Analogue to Digital Conversion (ADC) in a form a High and Low Signal Output. Micro – controller 4 will input the output of OP-AMP 11 and depending on the status of the FSR 13, green LED will light (which is an indication that 5V is sent to a camera for triggering it) or red LED will light (which means 0V is sent to a camera or in simple terms a camera is not triggered as it requires 5V to be trigged).

The programming code for triggering circuit.



```
int CAM_TRIG = 13;
int FSR = 12;
int GREEN_LED = 10;
int RED_LED = 9;
int FSR_STATE ;

void setup() {

    pinMode(CAM_TRIG, OUTPUT);
    pinMode(FSR, INPUT);
    pinMode(GREEN_LED, OUTPUT);
    pinMode(RED_LED, OUTPUT);

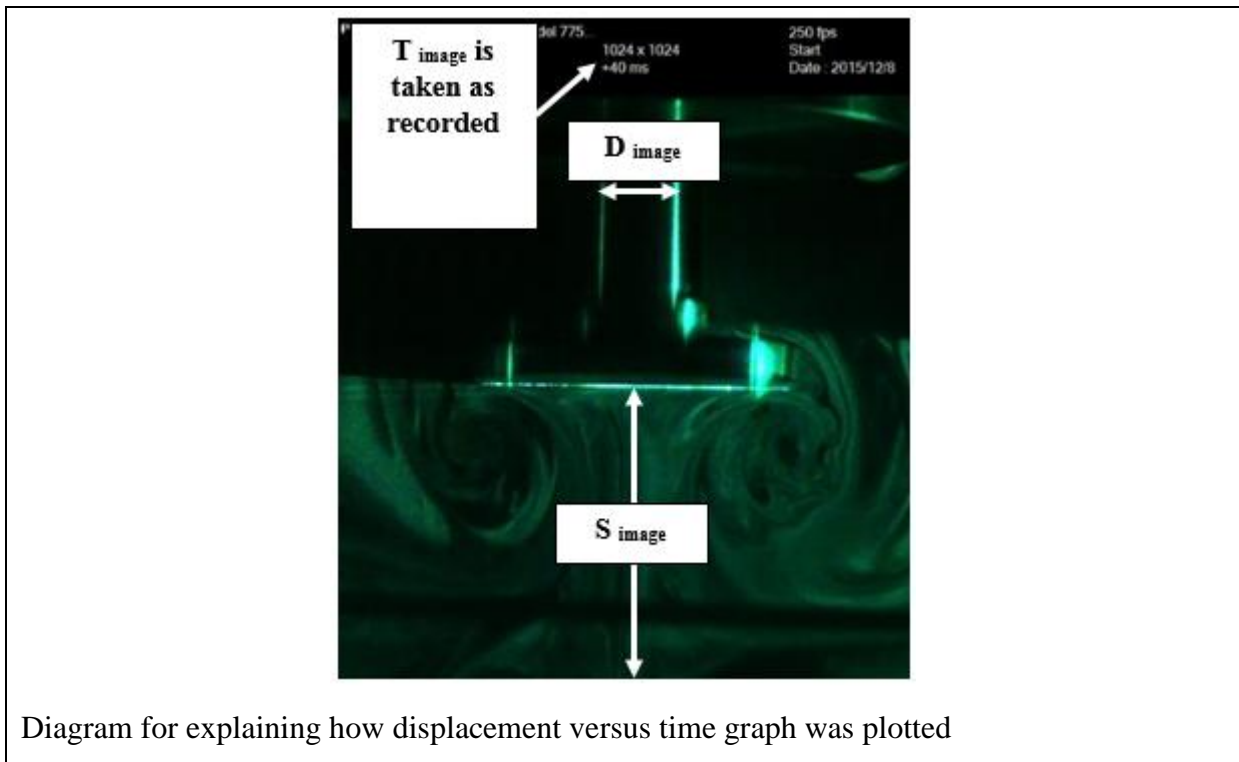
}

void loop()
{
    FSR_STATE = digitalRead(FSR);

    if(FSR_STATE == LOW)
    {
        digitalWrite(CAM_TRIG, HIGH);
        digitalWrite(GREEN_LED, HIGH);
        digitalWrite(RED_LED, LOW);
    }
    else
    {
        digitalWrite(CAM_TRIG, LOW);
        digitalWrite(GREEN_LED, LOW);
        digitalWrite(RED_LED, HIGH);
    }

}
```


Appendix 3: Estimating the acceleration



Converting displacement (S_{image}) on the image in to real displacement in the experiment (S)

$S = S_{image} \times \frac{D_{actual}}{D_{image}}$, where S is real displacement in the experiment, S_{image} is the displacement as measured from the image, D_{image} is the shaft diameter as measured from the image and D_{actual} is the actual diameter as measured in the experiment.

Table 11: Data for accelerating circular plate

Frame number	Displacement trials S(T)					Time T in (s)	Theoretical plate displacement in m	Plate velocity $V_p(T)$ in m/s	Reynolds number Re
	Test 1	Test 2	Test 3	Test 4	Average				
0	0.00000	0.00000	0.00000	0.00000	0.0000	0.000	0.0000	0.0	0
10	0.00000	0.00039	0.00000	0.00000	0.0001	0.001	0.0001	0.1	688
20	0.00000	0.00078	0.00039	0.00039	0.0004	0.003	0.0006	0.4	2063
30	0.00039	0.00078	0.00000	0.00078	0.0005	0.004	0.0010	0.5	2750
40	0.00078	0.00027	0.00078	0.00078	0.0007	0.006	0.0023	0.8	4126
50	0.00013	0.00052	0.00117	0.00156	0.0008	0.007	0.0031	0.9	4813
60	0.00132	0.00235	0.00235	0.00235	0.0021	0.009	0.0051	1.1	6189
70	0.00391	0.00391	0.00352	0.00489	0.0041	0.010	0.0064	1.3	6876
80	0.00547	0.00587	0.00547	0.00547	0.0056	0.011	0.0077	1.4	7564
90	0.00646	0.00782	0.00782	0.00782	0.0075	0.013	0.0107	1.7	8939
100	0.01107	0.01017	0.01017	0.01017	0.0104	0.014	0.0124	1.8	9627
110	0.01416	0.01329	0.01329	0.01416	0.0137	0.016	0.0163	2.0	11002
120	0.01603	0.01642	0.01642	0.01686	0.0164	0.017	0.0184	2.2	11690
130	0.02149	0.01955	0.02072	0.02033	0.0205	0.019	0.0229	2.4	13065
140	0.02307	0.02346	0.02346	0.02268	0.0232	0.020	0.0254	2.5	13752
150	0.02806	0.02737	0.02805	0.02659	0.0275	0.021	0.0280	2.7	14440
160	0.03231	0.03128	0.03128	0.03050	0.0313	0.023	0.0336	2.9	15815
170	0.03655	0.03597	0.03616	0.03441	0.0358	0.024	0.0366	3.0	16503
180	0.03974	0.04028	0.03988	0.03910	0.0398	0.026	0.0429	3.3	17878
190	0.04665	0.04497	0.04458	0.04427	0.0451	0.027	0.0463	3.4	18566
200	0.05084	0.05007	0.04888	0.04890	0.0497	0.029	0.0534	3.7	19941
210	0.05547	0.05474	0.05318	0.05388	0.0543	0.030	0.0572	3.8	20629
220	0.05661	0.05972	0.05787	0.05709	0.0578	0.031	0.0610	3.9	21316
230	0.06452	0.06413	0.06256	0.06203	0.0633	0.033	0.0692	4.2	22692

Equations used

$$Re(T) = \frac{\rho V_p(T) D}{\mu}$$

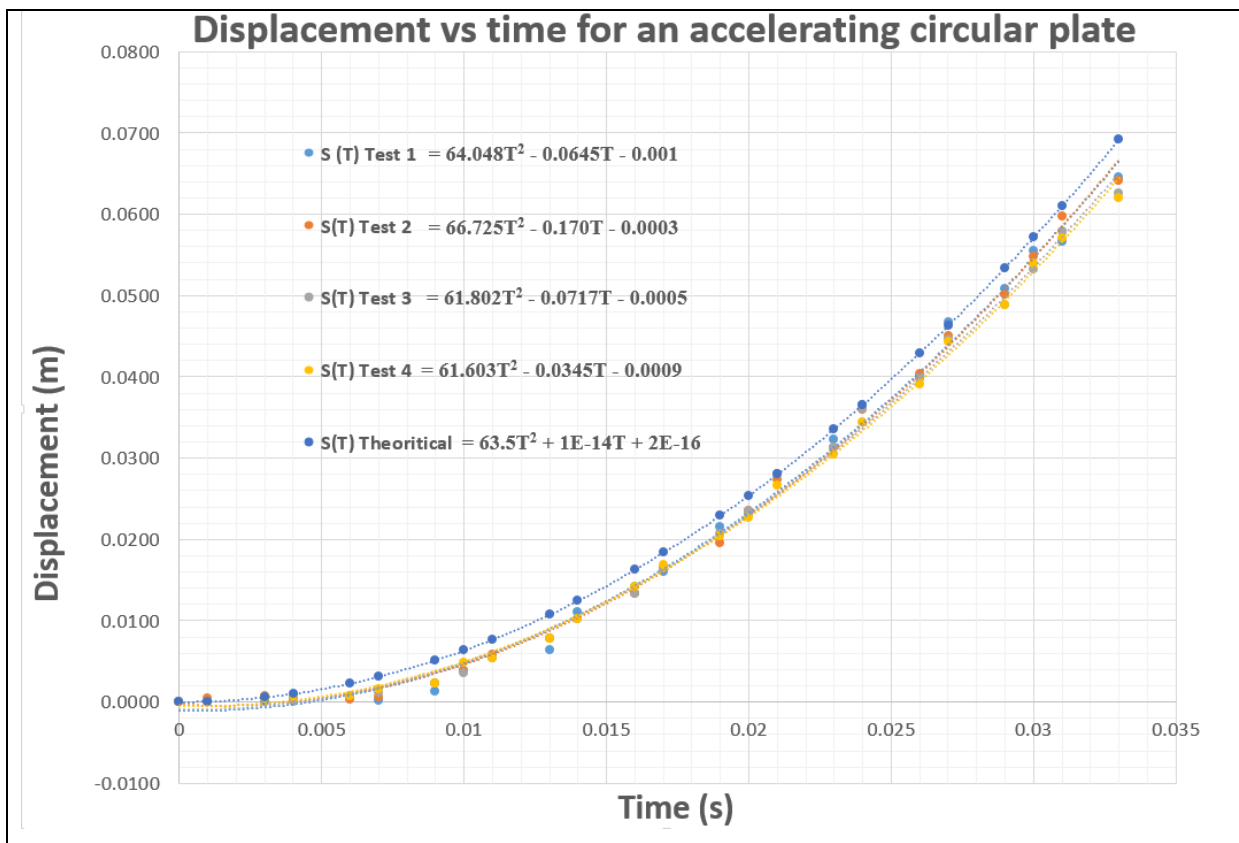
where Re is Reynolds number, ρ is the density of air (1.225kg/m³ at sea level and 15°C) $V_p(t)$ is the plate velocity in m/s at time T, D is diameter of the plate (0.08m) and μ is the dynamic viscosity (1.81x10⁻⁵ kg/(ms) at sea level and 15°C)

$$V_p(T) = a_p T$$

where $V_p(T)$ is the plate velocity at time T, a_p is the plate acceleration.

$$S(T) = 0.5a_p T^2$$

where S(T) is plate displacement at time T



Test	Function S(T) (m)	$\frac{d^2S}{dt^2} = \text{Acceleration (ms}^{-2}\text{)}$
1	$S(T) = 64.048T^2 - 0.0645T - 0.001$	128
2	$S(T) = 66.725T^2 - 0.170T - 0.0003$	133.4
3	$S(T) = 64.048T^2 - 0.0645T - 0.001$	128
4	$S(T) = 61.603T^2 - 0.0345T - 0.0009$	123.2
Theoretical	$S(T) = 64T^2 = 0.5a_p T^2$	127